8. SITE 1080[1]

Shipboard Scientific Party[2]

HOLE 1080A

Position: 16°33.5803′S, 10°49.2029′E

Start hole: 0407 hr, 7 September 1997

End hole: 1730 hr, 7 September 1997

Time on hole: 13.38 hr

Seafloor (drill pipe measurement from rig floor, mbrf): 2777.2

Total depth (drill pipe measurement from rig floor, mbrf): 2829.3

Distance between rig floor and sea level (m): 11.4

Water depth (drill pipe measurement from sea level, m): 2765.8

Penetration (mbsf): 52.1

Coring totals:

Type: APC
Number: 6
Cored: 50.8 m
Recovered: 55.5 m (109.2%)

Type: XCB
Number: 1
Cored: 1.3 m
Recovered: 0.12 m (9.2%)

Lithology:

Unit I: dark greenish gray to olive-gray, diatom-bearing and diatom-rich silty clays with varying abundances of nannofossils and foraminifers

HOLE 1080B

Position: 16°33.5963′S, 10°49.2043′E

Start hole: 1730 hr, 7 September 1997

End hole: 0600 hr, 8 September 1997

Time on hole: 12.50 hr

Seafloor (drill pipe measurement from rig floor, mbrf): 2779.3

Total depth (drill pipe measurement from rig floor, mbrf): 2817.5

Distance between rig floor and sea level (m): 11.4

Water depth (drill pipe measurement from sea level, m): 2767.9

Penetration (mbsf): 38.2

Coring totals:

Type: APC
Number: 4
Cored: 37.7 m
Recovered: 40.1 m (106.3%)

Type: XCB
Number: 1
Cored: 0.5 m
Recovered: 0.0 m (0.0%)

Lithology:

Unit I: dark greenish gray to olive-gray, diatom-bearing, and diatom-rich silty clays with varying abundances of nannofossils and foraminifers

Principal results: Site 1080, in the Southern Angola Basin, was selected to sample the northern end of the Angola-Namibia upwelling region. The site should complement results obtained from Site 1081 at the Walvis Ridge. It is not only important for reconstruction of the history of the Benguela Current and coastal upwelling migration, but also for its contribution to the climatic history of southern Africa. In addition to frequencies and phases of productivity variations, we expect to obtain information on dry–wet cycles in the drainage basin of the Kunene River. Of special interest in this context is the relationship of such cycles to the northern monsoon.

Two holes were cored with the advanced hydraulic piston corer (APC) at Site 1080 to a maximum depth of 52.1 meters below seafloor (mbsf), which recovered a hemipelagic sedimentary section probably spanning ~1 m.y. in the Pleistocene. Hole 1080A was cored with the APC to 50.8 mbsf and deepened with the extended core barrel (XCB) to 52.1 mbsf, with high torque and very little penetration in a very hard authigenic dolomite layer. Coring with the APC advanced at Hole 1080B to 37.7 mbsf when a hard dolomite layer resulted in no advance. An XCB core barrel advanced 0.5 m in 25 min of rotation and led to the decision to terminate the site.

Drilling at Site 1080 recovered sediments from one lithostratigraphic unit composed of moderately bioturbated, dark greenish gray to olive-gray, diatom-bearing, and diatom-rich silty clays with varying abundances of nannofossils and foraminifers. The clastic fraction is dominated by coarse silt-sized, angular, mono- and polycrystalline quartz grains with rare feldspar and detrital apatite clasts; smectite, kaolinite, and perhaps illite; the feldspar minerals albite and microcline; and muscovite. The biogenic component is represented by frequent diatom fragments, foraminifer fragments, and nannofossils. Radiolarians, plant remains, and particulate organic matter are present in trace amounts. Authigenic minerals include rounded glauconitic peloids and framboidal pyrite.

Detailed comparisons between the magnetic susceptibility and gamma-ray attenuation porosity evaluator (GRAPE) density records generated on the multisensor track (MST) and high-resolution color reflectance measured with the Minolta spectrophotometer demonstrated complete recovery of the sedimentary sequence down to 42 meters composite depth (mcd).

Micropaleontological studies were carried out on core-catcher samples from Holes 1080A and 1080B. The downhole succession of nannofossil assemblages from both holes suggests that the sedimentary sequence is incomplete and disturbed, possibly by turbiditic deposition. A hiatus of at least 400-k.y. duration (Zone NN20 and upper part of Zone NN19) was identified within a disturbed interval from 12 to 25 mbsf. Planktonic foraminifers are dominated by *Globigerina bulloides*, a species characteristic for upwelling and a high-productivity indicator. Dissolution effects increase downhole, reducing the abundance of the planktonic foraminifers. The absence of *Neogloboquadrina pachyderma* may represent a change to warmer surface-water conditions, but it may

[1]Wefer, G., Berger, W.H., Richter, C., et al., 1998. *Proc. ODP, Init. Repts.,* 175: College Station, TX (Ocean Drilling Program).

[2]Shipboard Scientific Party is given in the list preceding the Table of Contents.

also be an artifact of dissolution. Radiolarians are present throughout the section with an abundance that ranges from few to abundant. The preservation is good in all investigated samples, and no apparent reworking has been identified. Diatom abundance ranges from few to abundant. In general, preservation is poor, and diatom valves are fragmented. Silicoflagellates, opaline phytoliths, and sponge spicules are also present. Reworking is not evident. The presence of nonplanktonic diatoms in all core-catcher samples points to material derived from the shelf. Upwelling species dominate. *Chaetoceros* resting spores are abundant in all samples and are accompanied by neritic (rare–few) and open-ocean species (trace–rare).

A magnetostratigraphy was determined after alternating-field (AF) demagnetization at 20 mT. The Matuyama/Brunhes boundary is present in both holes at ~10 mbsf, and the onset and termination of the Jaramillo Subchron (C1r.1n) was identified at Hole 1080A at 51 and 41 mbsf, respectively. A short reversal event in the Matuyama Chron was identified at both holes. The relative shortness of the Brunhes Chron compared with the distance to termination of the Jaramillo Chron suggests that the upper Quaternary record is missing at this site.

Sediments average 2.4 wt% total organic carbon (TOC), which is rather high for ocean margin areas and reflects a history of elevated primary production in this area. Interstitial waters were gathered at a frequency of one sample per section, allowing high-resolution study of diagenetic processes through the entire cored sequence. The presence of a dolomite layer at 50 mbsf, which terminated drilling, indicates rock-forming dolomitization within the last 1 m.y. at this site. The profiles of alkalinity, ammonium, phosphate, and sulfate in the upper 10 mbsf reflect the degradation of organic matter, and the distributions of dissolved calcium, magnesium, and strontium indicate active calcite dissolution and dolomite formation. Throughout this upper interval, the concentration of sedimentary calcite decreases from 26 to <5 wt%, and dissolved strontium concentrations increase. From 25 mbsf to the dolomite layer, calcium and magnesium concentrations remain stable. The absence of decreases in these cations indicates that the dolomite layer is no longer growing.

Physical sediment properties were determined both by high-resolution MST core logging and index properties measurements. Magnetic susceptibility and GRAPE signals reveal characteristic cyclicities, which were used for high-quality stratigraphic correlation in conjunction with digital color data.

The original goal to obtain a high-resolution record of the northern end of the Angola-Namibia upwelling system was not achieved. Hard dolomite layers at a depth of 35 to 50 mbsf denied recovery by APC and proved difficult to penetrate by XCB, as well. Also, it was soon appreciated that the sedimentary sequence is incomplete at this site and that calcareous fossils have been largely dissolved below the upper portion of the sequence. We anticipate, nevertheless, interesting insights into the dynamics of the mid-Pleistocene climate revolution from this site, with an expanded section between the termination of the Jaramillo and onset of the Brunhes Chrons.

BACKGROUND AND OBJECTIVES

Site 1080 in the Southern Angola Basin was selected to sample the northern end of the Angola-Namibia upwelling region (Fig. 1). The site complements the Walvis Ridge Site 1081. Site 1080 should help reconstruct the history of the Benguela Current and coastal upwelling migration and also provide evidence of the climatic history of southern Africa. The Kunene River, which reaches the coast at ~17°S, is at the climatological barrier between the illite-rich zone in arid areas to the south and the kaolinite-rich zone characterized by tropical weathering areas to the north (Bornhold, 1973). Site 1080 is situated on a climatic boundary and should sensitively reflect changes in the position of continental climatic zones.

Of the various upwelling cells along the southwest African coast, the Kunene cell is the northernmost (Duncombe Rae et al., 1992; Fig. 1). It is of great interest to explore the relationship of this cell to those farther to the south, which (presumably) are, on average, more active. If, during cold pulses, the Benguela Current pushes north along the coast, the Kunene upwelling cell should be greatly stimulated and lead to increased supply of organic matter at Site 1080. If the Benguela Current turns westward during periods of intensification as proposed, the Kunene cell should remain subdued relative to the southern cells.

In addition to frequencies and phase of productivity variations, we expect to obtain information on dry–wet cycles in the drainage basin of the Kunene River. Of special interest in this context is the relationship of such cycles to the northern monsoon; that is, to what extent its influence dominates even this far south.

Stratigraphic data from two gravity cores (Geosciences Bremen [GeoB] 1023, water depth 1918 m; GeoB 1024-2, water depth 2799) show high Pleistocene sedimentation rates (10–50 cm/k.y.; Wefer et al., 1988; Schneider et al., 1992).

OPERATIONS

Hole 1080A (Proposed Site SAB-2)

After a 314-nmi voyage at an average speed of 10.7 kt, the vessel proceeded directly to the Global Positioning System coordinates of the site, where a beacon was deployed at 0407 hr on 7 September. Hole 1080A was spudded at 1020 hr on 7 September. The seafloor depth was established at 2765.8 meters below sea level (mbsl) by drill-pipe measurement (DPM). APC coring advanced to 50.8 mbsf (Table 1; also see the expanded core summary table on CD-ROM, back pocket, this volume), which was considered APC refusal when an attempt at the seventh piston core resulted in no advance because of contact with a very hard layer. Cores were oriented starting with Core 175-1080A-4H. The hole was then deepened with the XCB from 50.8 to 52.1 mbsf, with high torque and very little penetration. After 20 min of rotation, the core barrel was recovered containing 0.12 m of dolomite, and the hole was terminated. The bit cleared the seafloor at 1730 hr on 7 September.

Hole 1080B

The vessel was offset 40 m to the south, and Hole 1080B was spudded with the APC at 1845 hr. The seafloor depth was established at 2767.9 mbsl by DPM. APC coring advanced to 37.7 mbsf. When the attempt at Core 175-1080B-5H resulted in no advance of the core barrel because of a hard sediment layer, an XCB core barrel was dropped (5X) and advanced 0.5 m in 25 min of rotation. The decision was made to terminate the site, and the drill string was pulled back to 2767.0 m, clearing the seafloor at 0025 hr on 8 September. The hydrophones and thrusters were retracted, and the drilling equipment was secured for transit by 0600 hr, thereby ending operations at Site 1080.

SITE GEOPHYSICS

Introduction and Strategy

The third working area of Ocean Drilling Program (ODP) Leg 175 was in the northern part of the Angola-Namibia coastal upwelling cell (Schell, 1970; Nelson and Hutchins, 1983; Stramma and Peterson, 1989), which also represents the northernmost extent of the modern trade-wind-driven upwelling in this area. The region is located at ~17°S between the Mid-Angola Basin Sites 1078 and 1079 and the Walvis Ridge.

The early opening of the South Atlantic in the Walvis Ridge area is supposed to be of Late Jurassic age according to Sibuet et al. (1984). It was accompanied by crustal thinning, development of basaltic wedges of seaward-dipping reflectors, and blockfaulting. In

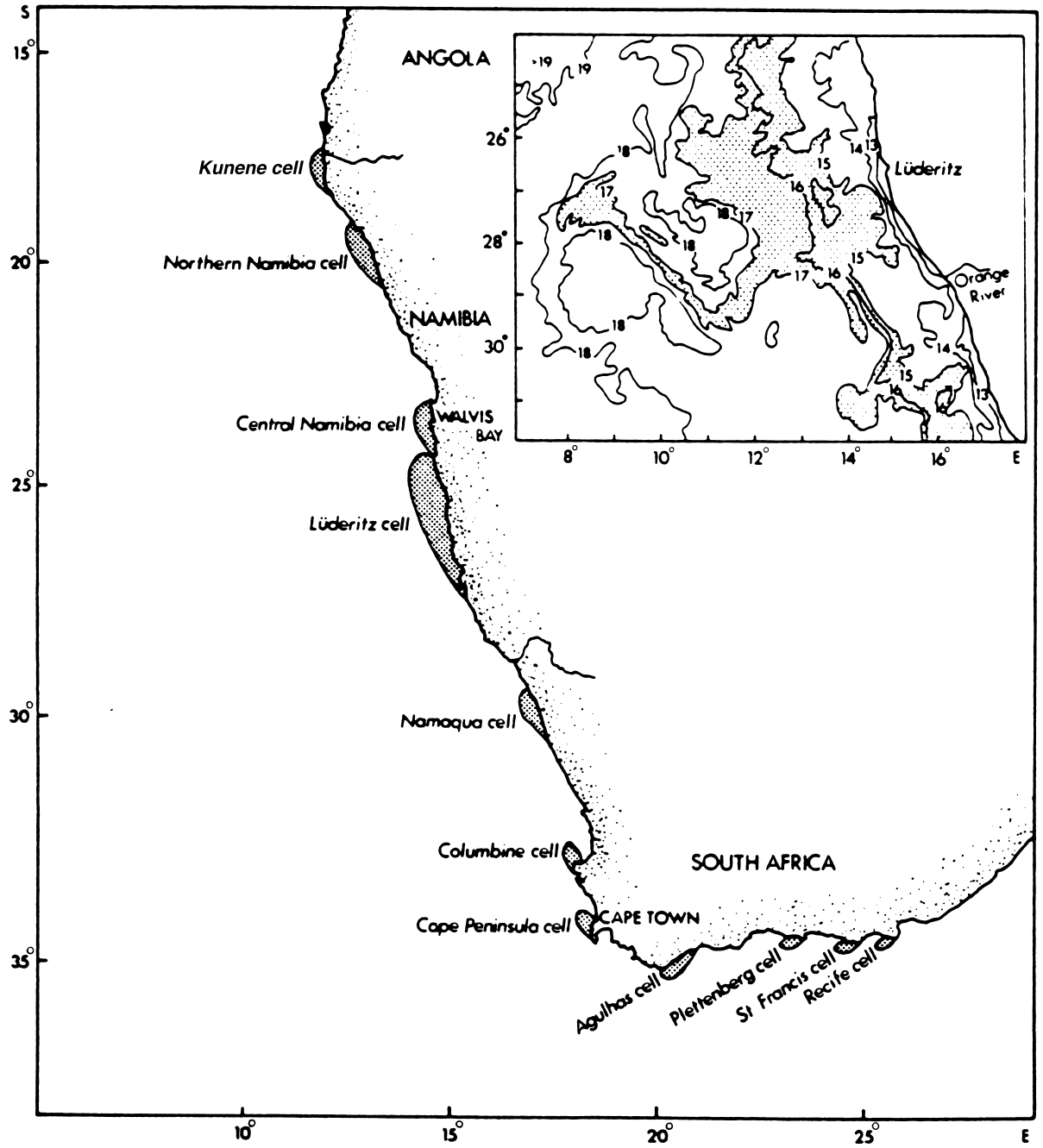

Figure 1. Principal upwelling cells in the Benguela Current system and the Agulhas Bank. Inset shows surface isotherms for 15 June 1989, with cool frontal water (shaded) entrained around the Agulhas Ring (modified after Duncombe Rae et al., 1992). Site 1080 is located north of the Kunene cell.

Aptian–Albian times, an eastward ridge jump occurred (Cande and Rabinowitz, 1978; Kumar, 1979), which placed part of the original African continental margin in this area onto the South American Plate. Accordingly, the continental margin closest to Site 1080 is rather narrow with steep slopes, resulting in downslope sediment transport by slides, debris flows, and turbidity currents (Embley and Morley, 1980). The morphology is further complicated by sedimentary tectonism and giant sediment slides. Thus, a well-defined pelagic depositional pattern could be identified only in a few places at this site.

As multiple major and minor slides are documented in the survey region, highest priority was given to the identification of areas with an apparently undisturbed sedimentation. Because of the generally steep slopes, the most promising depth ranges were expected in the mid and lower stretches of the continental margin. The initial seismic line was oriented along an earlier Parasound profile (*Meteor* Cruise M20/2), which had revealed undisturbed near-surface sediments in a number of places. Only two suitable drill sites could be identified in water depths between 2200 and 3000 m and were crossed by additional seismic lines. All areas shallower than 2200 m and deeper than 3000 m were found to be affected by intensive slumping.

The seismic characteristics are summarized here for the cored interval at Site 1080. The bathymetric records confirm the complex nature of the depositional environment, and it became clear from the

Table 1. Coring summary for Site 1080.

Core	Date (Sept 1997)	Time (UTC)	Interval (mbsf)	Length cored (m)	Length recovered (m)	Recovery (%)
175-1080A-						
1H	7	1035	0.0-3.3	3.3	3.35	101.5
2H	7	1120	3.3-12.8	9.5	9.90	104.2
3H	7	1155	12.8-22.3	9.5	10.38	109.3
4H	7	1250	22.3-31.8	9.5	11.05	116.3
5H	7	1350	31.8-41.3	9.5	10.75	113.2
6H	7	1435	41.3-50.8	9.5	10.02	105.5
7X	7	1700	50.8-52.1	1.3	0.12	9.2
Coring totals:				52.1	55.57	106.7
175-1080B-						
1H	7	1905	0.0-9.2	9.2	9.22	100.2
2H	7	1955	9.2-18.7	9.5	9.63	101.4
3H	7	2050	18.7-28.2	9.5	10.26	108.0
4H	7	2140	28.2-37.7	9.5	10.95	115.3
5X	7	2355	37.7-38.2	0.5	0.00	0.0
Coring totals:				38.2	40.06	104.9

Notes: UTC = Universal Time Coordinated. An expanded version of this coring summary table that includes lengths and depths of sections and comments on sampling is included on CD-ROM (back pocket, this volume).

combined Hydrosweep and Parasound echosounder data sets that very few potential drill sites may be found in the region. Some locations are apparently better protected from mass movements by the local topography, perhaps featuring an underlying basement high.

The selection of drill sites in the Angola-Namibia upwelling region also was based on digital Parasound data. They allowed a clear distinction between chaotic and regular sediment structures on a meter scale. Seismic data commonly showed a continuous layering, whereas the Parasound system imaged a microtopography with rough, scattering surfaces. The signal penetration, on the order of 50 to 75 m, was generally lower than in the survey areas farther north, possibly because of lower clay and higher silt and sand concentrations, which may indicate higher proportions of coarse-grained shelf materials transported downslope. The selected drill sites showed regular seismic patterns of layered sediment structures, which should represent a continuous and primarily hemipelagic sedimentation, possibly intercalated with turbidites and thin mass-flow deposits. Occasionally, small hyperbolic echoes suggest undulating surfaces or a rough microtopography that cannot be distinguished because of the limited resolution of the seismic data. Because the frequency band of the seismic source, as well as the recording system, extends to several hundred hertz, a comparatively detailed image of the sedimentary structures is provided. If only the frequency band below 100 Hz had been considered—as for usual multichannel seismic surveys—the reflection pattern would appear much more regular.

Seismostratigraphy

Altogether, six seismic lines were shot in the working area (Fig. 2; Bleil et al., 1995), with Line GeoB 93-031 lying slightly north of Line 40 of Emery et al. (1975), where the originally proposed site was located. It was obvious from these old data that new locations with less disturbed or undisturbed sedimentary sequences had to be found to carry out high-resolution paleoceanographic studies. In addition to these lines, seven seismic lines were shot across Deep Sea Drilling Project (DSDP) Site 530 (Hay, Sibuet, et al., 1984) in the southernmost Angola Basin and DSDP Site 532 (Hay, Sibuet, et al., 1984) on the Walvis Ridge with equally high resolution for a direct comparison with the working area (Fig. 2). These data provide a basis for a seismostratigraphic framework making use of pronounced similarities of the seismic characteristics, which is under development. The two proposed sites SAB-1 and SAB-2 lie on Line GeoB/AWI 93-030 (Fig. 3), which also revealed large vertical scarps from slope failures (e.g., at common depth points [CDP] 3250, 3750, or 4000), or slump deposits at the surface from CDP 1600 to 1750.

Penetration of the seismic signal was generally much higher here than at the northern sites, indicating the absence of attenuating gas charges and allowing the development of a seismostratigraphic concept down to 8 s two-way traveltime (TWT). Coring was originally planned for 600-m penetration, but only 52 m of the sediment column were recovered from Site 1080 because of the presence of lithified dolomitic layers. Therefore, sediments were retrieved only from the uppermost seismic unit, which is characterized by numerous continuous, distinct parallel reflectors of high amplitude, partly disrupted by minor vertical faulting (Fig. 3). The base of the unit is marked by a prominent, discontinuous high-amplitude reflector, which is associated with a significant decrease in overall reflection amplitudes and signal frequency at depth. In contrast to all deeper lying units down to 3 s TWT sub-bottom depth, this unit shows a remarkable thickening toward the coast from ~100 m at the western end of Line GeoB/AWI 93-030 to ~450 m. This is not typical for a depositional style dominated by turbiditic sediments, but for hemipelagic sediment input with a source close to the shore. Therefore, biogenic sediments resulting from coastal upwelling and terrigenous sediment from the shelf (and ultimately from the Kunene River) are tentatively identified as the dominating sediment sources.

Compared with proposed site SAB-1 (Fig. 3), a sediment package of ~50 m thickness is missing at Site 1080. It could not be determined from the seismic data whether this package at SAB-1 was derived from a slumped deposit or overlying normal sediments, or whether it is truly missing at Site 1080. The local and small-scale disturbances in the sedimentary sequences seen in the record will presumably complicate interpretation of the drilling results. Nevertheless, the selected sites are among the very few places in the area with a reasonably clear, parallel reflector pattern, which should greatly facilitate the reconstruction of the regional sedimentation history.

Site 1080

Site 1080 is located in 2766 m water depth at the northeastern end of the survey area on Line GeoB/AWI 93-030 (CDP 2156). Figure 4 shows a 10-km-long seismic section of Line GeoB/AWI 93-030 across Site 1080. The sedimentary sequence appears largely undisturbed, with some minor faulting. Some horizons with diffractions indicate rough interfaces (e.g., top of slump units). Most reflectors show a pronounced continuity, as is known from hemipelagic or turbiditic sequences. Reflectivity decreases beneath 300 ms TWT, with a gradual transition to a mostly transparent unit. The origin of the contrast between this transparent unit and the high-amplitude reflections in the upper unit is unknown, but it must represent significant differences in physical properties.

Figure 5 shows a close-up of the seismic section over a 1-km-long interval near the drill site, plotted against sub-bottom depth for a sound velocity of 1500 m/s. Seismic reflectors are compared with the wet bulk density data for Hole 1080A, derived from index properties measurements (see “Physical Properties” section, this chapter), which show some pronounced variations. Seismograms are plotted as wiggle traces with gray-scaled amplitudes as background. Density, which mostly controls changes in acoustic impedance at shallow depth, reveals marked physical and lithologic changes that should be visible in the seismic records. All changes identified could be assigned to individual seismic reflectors; however, verification will come from postcruise modeling.

Dolomitic layers were found at 52 mbsf at Hole 1080A and at 38 mbsf at Hole 1080B, where drilling was stopped. At both holes, a continuous, high-amplitude reflector is observed, which could result from the presence of dolomite as a continuous layer. A nodular distribution could be generating the reflector, but reflection amplitudes would be reduced (depending on the density of the nodules). Because

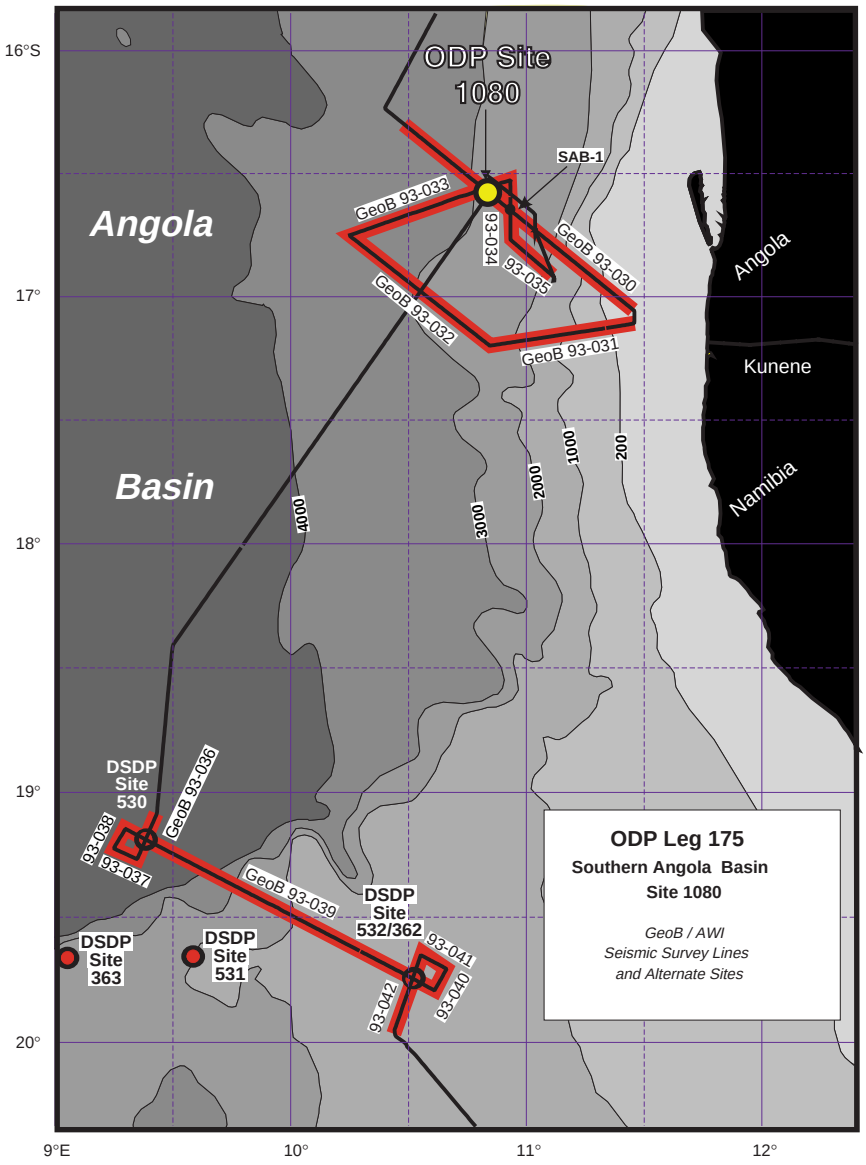

Figure 2. Map of seismic presite survey lines, proposed site locations, ODP Leg 175 drill Site 1080 in the Southern Angola Basin, and DSDP Sites 530 and 532. Bathymetry was derived from Gebco Digital Dataset on CD-ROM.

thin layers have seismic attributes different from those of normal reflectors, further shore-based analysis could shed some light on the areal pattern of dolomitization.

LITHOSTRATIGRAPHY

Introduction

Two holes (A and B) were drilled at Site 1080. Hole 1080A was drilled to a maximum depth of 50.8 mbsf before an authigenic dolomite horizon prevented further drilling (see "Operations" section, this chapter). Hole 1080B was also abandoned after intersecting a dolomite horizon at 37.7 mbsf. Moderate core disturbance is common in the top of Section 1 of all cores. Cores 175-180A-4H through 6H are intensely disturbed from the rapid expansion of gas.

Description of Lithostratigraphic Unit

Sediments from Site 1080 form one lithostratigraphic unit composed of moderately bioturbated, dark greenish gray (5GY 4/1) to olive-gray (5Y 4/2), diatom-bearing, and diatom-rich silty clays with varying abundances of nannofossils and foraminifers. Diffuse, dark gray color bands, 0.5 cm thick, composed of framboidal pyrite are present in intervals 175-1080A-5H-1, 48–76 cm, and 5H-2, below 100 cm. Rare, whitish gray nodules, 1–2 mm in diameter, are disseminated throughout Cores 175-1080A-4H through 6H and Cores 175-1080B-1H through 3H.

Synthesis of Smear-Slide Analyses

Smear-slide analyses indicate that silty clay is the dominant lithology at Site 1080. The clastic fraction is dominated by coarse silt-sized, angular, mono- and polycrystalline quartz grains with rare subangular feldspar and detrital apatite clasts. Muscovite and biotite also are present in trace amounts. The biogenic component is represented by frequent diatom fragments, foraminifer fragments, and nannofossils. Radiolarians, plant remains, and particulate organic matter are present in trace amounts. Authigenic minerals include rounded glauconitic peloids and framboidal pyrite. Some glauconite grains contain euhedral pyrite grains, indicating secondary consumption of iron to form pyrite. Examination of a smear slide made from a whitish gray

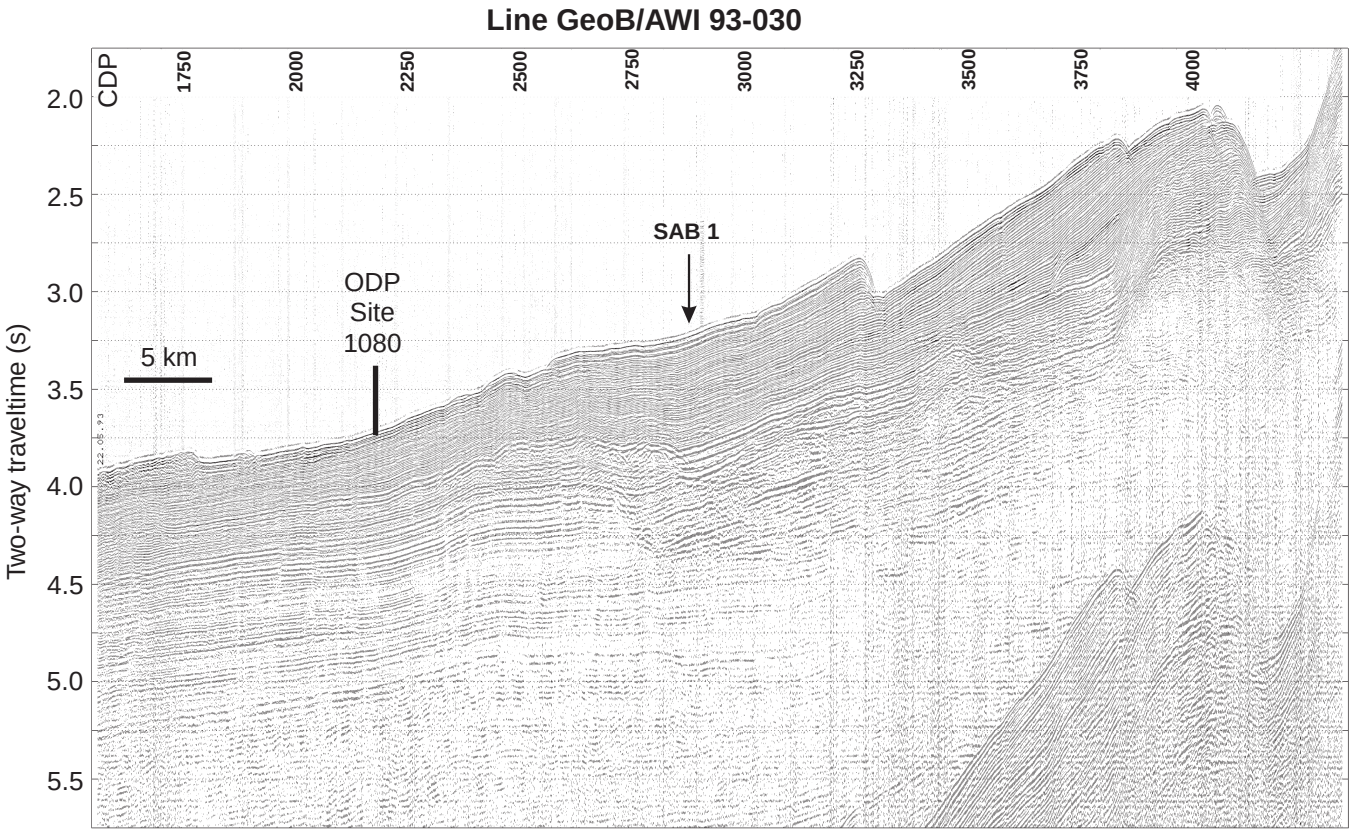

Figure 3. Seismic Line GeoB/AWI 93-030 with Site 1080. Proposed site SAB-1 is denoted by an arrow. Vertical axis is given in two-way traveltime. CDP interval is 25 m for a shotpoint spacing of 25 m. Seismic data is 24-fold stacked and not migrated. Site 1080 is located at CDP 2156.

nodule from Core 175-1080A-4H reveals that the nodules are composed entirely of sponge spicules and diatom fragments.

X-ray Diffraction Analysis

X-ray diffraction (XRD) analysis of sediments from Hole 1080A reveals that the clastic fraction is dominated by smectite, kaolinite and perhaps illite, quartz, the feldspar minerals albite and microcline, and muscovite. Pyrite is present as an accessory mineral in all samples. No clear identification could be made for other accessory phases. The smectites are generally poorly crystallized. The XRD patterns do not indicate the presence of dolomite.

Spectrophotometry

Color reflectance was measured, but because of the extensive core disturbance at this site, no discernable stratigraphic pattern was found either in the total reflectance or the red/blue ratio (Figs. 6, 7). The red/blue ratio, however, follows the general trend of the carbonate concentration (see "Inorganic Geochemistry" section, this chapter). In the top 10 mbsf, there is a high red/blue ratio (average of 1.4) and the carbonate concentration varies between 6 and 26 wt%. Below 10 mbsf, the red/blue ratio is lower (average of 1.15), and the carbonate concentration varies between 1.5 and 6 wt%.

BIOSTRATIGRAPHY AND SEDIMENTATION RATES

Site 1080 was drilled in 2800 m water depth in the Angola Basin. Sediment recovered from Site 1080 represents a disturbed and incomplete hemipelagic section, which terminates within the early–middle Pleistocene. The micropaleontological studies were carried out on core-catcher samples from Holes 1080A and 1080B. Additional samples from within the cores were examined for calcareous nannofossil-, diatom-, and silicoflagellate-based biostratigraphy.

Calcareous Nannofossils

Calcareous nannofossils were examined in core-catcher samples from Holes 1080A and 1080B. Additional samples within a disturbed sequence of Section 175-1080A-2H-5 were analyzed for identifying a possible sedimentary hiatus.

The downhole succession of nannofossil assemblages from both Holes 1080A and 1080B suggests that the sedimentary sequence is incomplete and disturbed by possible turbiditic deposition. Site 1080 terminated within the middle part of Zone NN19 (between 0.6 and 1 Ma), as shown by the dominance of Small *Gephyrocapsa* spp., the presence of *Pseudoemiliania lacunosa*, and the absence of *Helicosphaera sellii* in assemblages from the deepest samples.

Samples 175-1080A-1H-CC and 175-1080B-1H-CC are placed within Zone NN21b (younger than 0.09 Ma). The Zone NN21b/NN21a boundary lies between Samples 175-1080A-1H-CC and 2H-5, 44 cm. Zone NN21a is interrupted by a disturbed sequence located at Hole 1080B between the lower half of Core 175-1080B-2H and the upper half of Core 3H, and at Hole 1080A from Sample 175-1080A-2H-5, 49 cm, down to the upper part of Core 4H. Nannofossil assemblages within this disturbed sequence show abundant Pleistocene reworking. Abundant aragonite needles within the upper part of this interval suggest rapid burial linked with turbiditic deposition. The lower part of Site 1080, immediately below the disturbed sequence, is placed in the lower part of Zone NN19. Hole 1080B terminated between 0.6 and 0.83 Ma (i.e., within the Small *Gephyrocapsa* acme

Zone sensu Weaver [1993]). Barren samples at the bottom of the deeper Hole 1080A prevented us from estimating a maximum age for this hole. Paleomagnetism suggests penetration to the Jaramillo Chron (see "Paleomagnetism" section, this chapter).

Planktonic Foraminifers

Planktonic foraminifers were examined from Holes 1080A and 1080B. Sample 175-1080A-1H-CC (3.25 mbsf) is dominated by *Globigerina bulloides* (an upwelling, high-productivity indicator) and also contains abundant *Neogloboquadrina pachyderma*. *Globorotalia inflata, Globorotalia crassaformis*, *Globorotalia scitula*, and *Globigerinita glutinata* are common, although not abundant, components of the fauna. *N. pachyderma* is an important species in the modern Benguela Current system (Little et al., 1997), and the sinistral form is found in association with coastal upwelling centers. *G. bulloides* is found in abundance in the fringes of the upwelling cells (Little et al., 1997). *G. inflata* is common in the transitional zone between upwelled water and subtropical waters and may function as an indicator of this boundary downcore. Unfortunately, dissolution affects the abundance of the planktonic foraminifers downcore. Samples 175-1080A-2H-CC and 4H-CC through 6H-CC are barren of planktonic foraminifers. Sample 175-1080A-3H-CC has rare foraminifers: *G. bulloides* and *G. crassaformis* are dominant, and *Globigerinoides ruber* is abundant. The absence of *N. pachyderma* may represent a change to warmer surface-water conditions, but it may also be an artifact of dissolution. There are no planktonic foraminifers in the 150- to 250-µm fraction.

A lithologic change associated with the Brunhes/Matuyama boundary in Core 175-1080A-2H-5 was subsampled and analyzed (Samples 175-1080A-2H-5, 43–45, 62–64, 70–72, and 103–105 cm). The presence of clay layers between the samples at 43 and 64 cm, 64 and 70 cm, and 70 and 103 cm suggests turbiditic deposition. There is a low planktonic/benthic foraminiferal ratio in the sample above the interval (Sample 2H-5, 43–45 cm). *G. inflata* and *G. bulloides* are dominant, and *G. crassaformis* is present. Sample 175-1080A-2H-5, 62–64 cm, is dominated by *G. inflata* and *N. pachyderma* (sinistral), with common *G. crassaformis*. *G. bulloides* is present but not abundant. This assemblage is different from others observed in the region and may represent reworking (i.e., mixed assemblages representing turbidite deposition). Sample 175-1080A-2H-5, 70 cm, is dominated by *G. bulloides* and *G. inflata*. *G. crassaformis* is present, but *N. pachyderma* (sinistral) is not. This fauna is similar to the sample immediately above the turbidite layer (Sample 175-1080A-2H-5, 43–45 cm) and is probably in situ. The lowermost sample (2H-5, 102 cm) is strongly affected by dissolution.

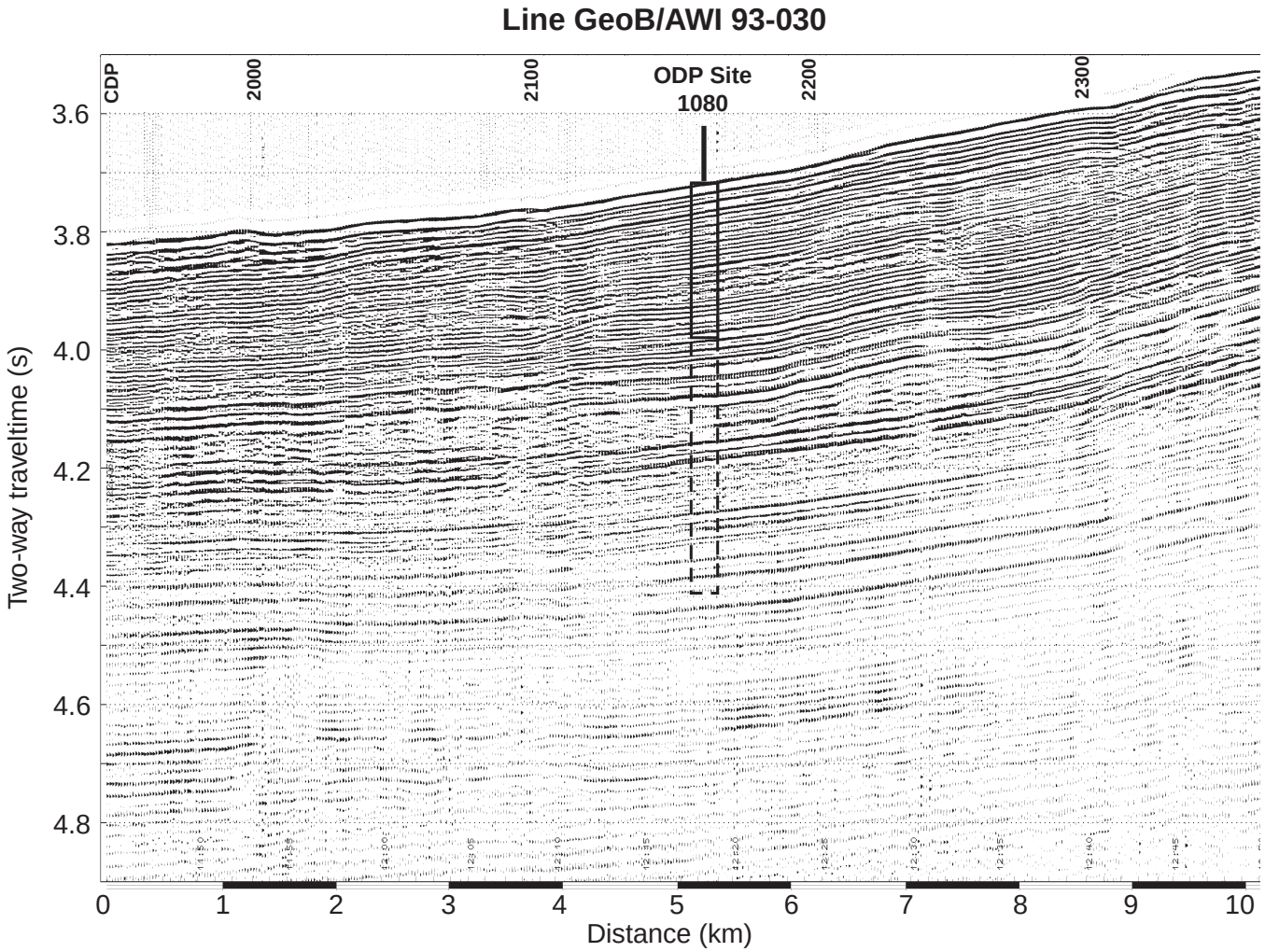

Figure 4. Seismic section of line GeoB/AWI 93-030 at Site 1080. Vertical axis is given in two-way traveltime. CDP interval is 25 m for a shotpoint spacing of 25 m. Site 1080 is located at CDP 2167. The box indicates the approximate penetration of the borehole of 200 m (APC) and 600 m (XCB), respectively.

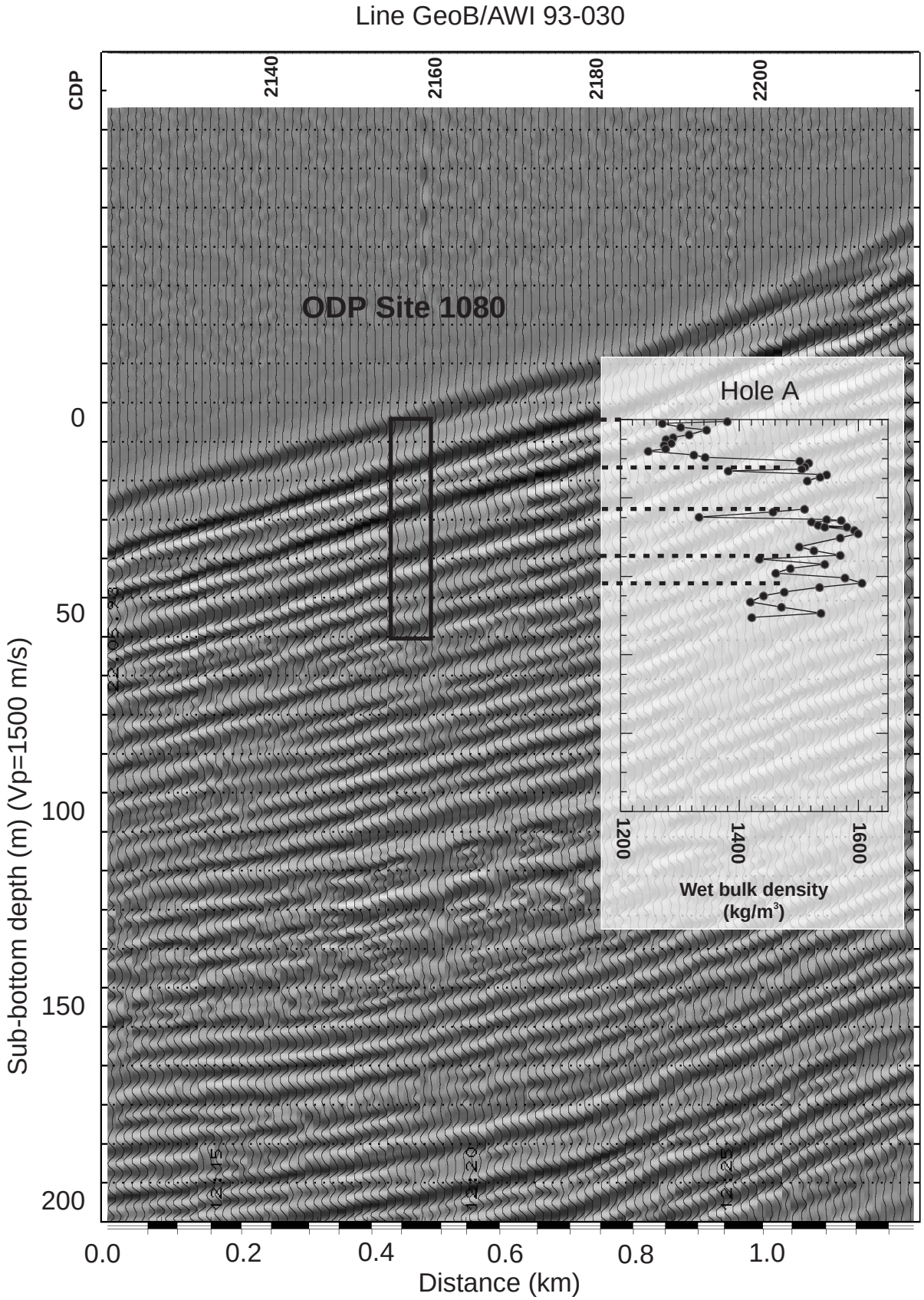

Figure 5. Close-up of Line GeoB/AWI 93-030 near Site 1080. Amplitudes are grayscaled. For comparison, wet bulk density data from index properties measurements are shown, and main reflectors are correlated with local extremes in the density log (dashed lines). For depth determination, a sound velocity (V_p) of 1500 m/s was used.

Benthic Foraminifers

The benthic foraminifers from Site 1080 were studied at both Holes 1080A and 1080B. The abundance is high in the first core catchers (Samples 175-1080A-1H-CC, 175-1080B-1H-CC, and 1080B-2H-CC). The subsequent core catchers are barren or contain very few benthic foraminifers. The preservation is good in the uppermost core catchers but deteriorates downhole.

The uppermost core catchers (Samples 175-1080A-1H-CC and 175-1080B-1H-CC) are dominated by *Nonion* sp. 1 (Table 2). Additional species are *Melonis barleeanum* and *Oridorsalis umbonatus*. The subsequent core catchers are dominated by *Bulimina exilis* with additional contribution from fissurinas, stilostomellas, uvigerinids, and the *Praeglobobulimina/Globobulimina* group. The lowermost two core catchers in each hole are barren (Samples 175-1080A-5H-CC and 6H-CC, and 175-1080B-3H-CC and 4H-CC, respectively).

Radiolarians

Radiolarians are present in all core-catcher samples from Hole 1080A (Table 3). Radiolarian abundance ranges from few to abundant, and preservation is good in all investigated samples. No apparent reworking has been identified.

Radiolarian fauna indicates a Quaternary age for Hole 1080A. The absence of *Axoprunum angelinum* suggests that the uppermost core (175-1080A-1H-CC) is within either the Pleistocene *Collosphaera tuberosa* Zone or the Pleistocene to Holocene *Buccinosphaera invaginata* Zone of Moore (1995).

Although the diagnostic species *Anthocyrtidium angulare* is absent throughout Hole 1080A, Samples 175-1080A-2H-CC, 3H-CC, and 4H-CC are assigned to the Pleistocene *A. angelinum* Zone or *Amphirhopalum ypsilon* Zone of Moore (1995) based on the presence of *A. angelinum* and the absence of *Lamprocyrtis neoheteroporos*. The diagnostic species *C. tuberosa*, which is used to recognize the *A. angelinum* and *A. ypsilon* Zones, is absent from the samples investigated. A last occurrence (LO) of *L. neoheteroporos* is found in Sample 175-1080A-5H-CC, indicating an age older than 1.07 Ma for the deeper two Samples 175-1080A-5H-CC and 6H-CC (Fig. 8).

Diatoms

Diatom analysis was carried out on smear slides of core-catcher samples from Holes 1080A and 1080B. Diatom abundance ranges from few to abundant. In general, preservation is poor, and diatom valves are fragmented. Silicoflagellates, opaline phytoliths, and sponge spicules are also present. Reworking is not evident. However, the presence of nonplanktonic diatoms in all core-catcher samples points to material advected from the shelf. The upwelling assemblage dominates. *Chaetoceros* resting spores are abundant in all samples and are accompanied by neritic (rare–few) and open-ocean species (trace–rare).

Samples 175-1080A-1H-CC and 175-1080B-1H-CC are assigned to the diatom *Pseudoeunotia doliolus* Zone; all other samples are assigned to the *Nitzschia rheinholdii* Zone.The silicoflagellate biostratigraphic marker, *Bachmannocena quadrangula* (LO, 0.8 Ma.; Locker, 1996), is found in Samples 175-1080A-2H-6, 80 cm, and 175-1080B-2H-3, 30 cm, which agrees with paleomagnetic data (Fig. 8; see "Paleomagnetism" section, this chapter).

PALEOMAGNETISM

The investigation of magnetic properties at Site 1080 included the measurement of bulk susceptibility of whole-core sections and the natural remanent magnetization (NRM) of archive-half sections. The Tensor tool was used to orient Cores 175-1080A-4H, 5H, and 6H and Cores 175-1080B-3H and 4H (Table 4).

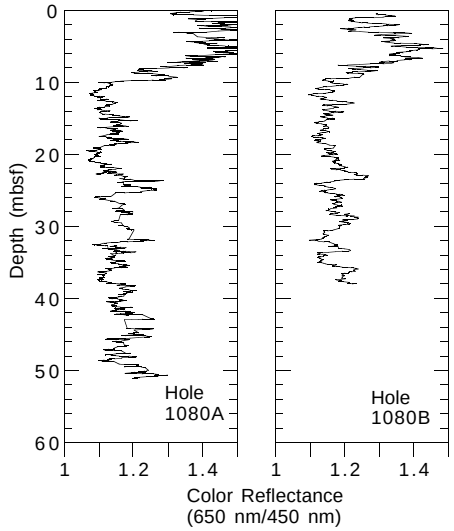

Figure 6. Downcore variation in the ratio of the red (650 nm) to blue (450 nm) wavelengths at Holes 1080A and 1080B. A nine- and five-point smoothing procedure was applied to the data sets for Holes 1080A and 1080B, respectively.

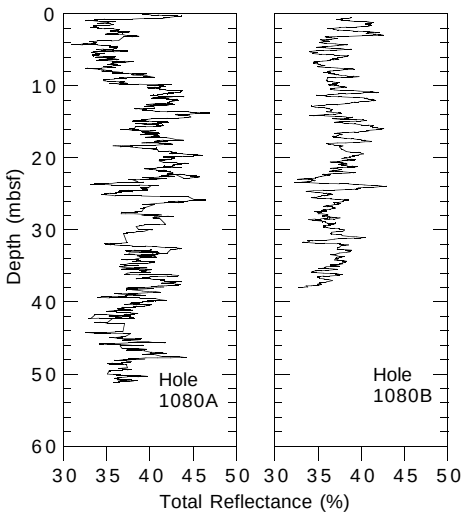

Figure 7. Downcore variation in the total reflectance of visible light (400–700 nm) at Holes 1080A and 1080B. A nine- and five-point smoothing procedure was applied to the data sets for Holes 1080A and 1080B, respectively.

Natural Remanent Magnetization and Magnetic Susceptibility

Magnetic susceptibility measurements were made on whole cores from both holes as part of the MST analysis (see "Physical Properties" section, this chapter). The magnetic susceptibility generally ranges from 1 to 15×10^{-5} (SI volume units; Fig.9).

Measurements of NRM were made on all archive-half core sections from Holes 1080A and 1080B. Sections from Hole 1080A were demagnetized by AF at 10 and 20 mT, and sections from Holes 1080B were demagnetized by AF at 20 mT only.

A primary magnetic component was preserved in sediments from Holes 1080A and 1080B, which allowed the determination of the magnetic polarity. Most of the magnetic overprint could be removed by 20-mT demagnetization, except for below ~40 mbsf at Hole 1080A, where the relatively large scatter of directions suggests the

Table 2. Relative abundance of benthic foraminiferal species and overall abundance of benthic foraminifers at Holes 1080A and 1080B.

Core, section, interval	Depth (mbsf)	Abundance	*Bolivina seminuda*	*Bolivina* sp. 1	*Bolivina* sp. 2	*Bulimina aculeata*	*Bulimina exilis*	*Bulimina mexicana*	*Cassidulina laevigata*	*Cassidulina minuta*	*Cassidulinoides* cf. *bradyi*	*Chilostomella ovoidea*	*Cibicidoides wuellerstorfi*	*Cibicidoides* sp. 1	*Eggerella bradyi*	*Epistominella exigua*	*Fissurina* spp.	*Frondicularia* sp. 1	*Fursenkoina fusiformis*	*Fursenkoina* sp. 1	*Gyroidinoides soldanii*	*Hyalinea balthica*	*Melonis barleeanum*	*Nodosaria* spp.	*Nonion* sp. 1	*Nonionella turgida*	*Oolina* spp.	*Oolina hexagona*	*Oridorsalis umbonatus*	*Praeglobobulimina/Globobulimina* group	*Pullenia bulloides*	*Pullenia subcarinata*	*Pyrgo* spp.	*Quadrimorphina allomorphinoides*	*Quinqueloculina* sp.1	*Sphaeroidina bulloides*	*Stilostomella* spp.	*Triloculina tricarinata*	*Uvigerina auberiana*	*Uvigerina hispidocostata*	*Uvigerina peregrina*	Unidentified	Number of specimens counted
175-1080A-																																											
1H-CC	3.25	A	3			+	+		4	3				+		+	2		+	+	+		7		54	5	+	+	5		1	+	+			4	+		+	+	+	3	3	518
2H-CC	13.15	R					25													2		2	2		2			2	32		3					3		2	7	6	14	59
3H-CC	23.13	F	2				7	1		6	+			9	3	1	5	2	5	2				+	2	+		+	9	13	1	1	1	2	+		5		3	2	+	13	172
4H-CC	34.07	R	2				25	4							4		10	10			2		4							2			2				10		12	2	10	4	52
5H-CC	42.50	B																																									0
6H-CC	51.27	B																																									0
175-1080B-																																											
1H-CC	9.17	C	3	+	2		2		9	3		+	2	2	1		4		2	+	+		18		23	1	+	+	8	+	2	4			2	5						4	170
2H-CC	18.78	C			+		52		+		18					+	8	2		+	+		+					+	+	1						7		1	2	1	3	228
3H-CC	28.91	B																																									0
4H-CC	39.10	B																																									0

Notes: The relative abundance of benthic foraminiferal species is given as a percentage, where + = <1%. Absolute abundance (per ~20 cm^3 of sediment) of benthic foraminifers is given as A = abundant (>500 specimens); C = common (250–500 specimens); F = few (100–249 specimens); R = rare (50–99 specimens); and B = barren (no specimens).

Table 3. Stratigraphic distribution of radiolarians at Hole 1080A.

Age	Zone	Core, section, interval	Depth (mbsf)	Abundance	Preservation	*Cycladophora cornutoides*	*Cycladophora davisiana*	*Eucyrtidium acuminatum*	*Lamprocyclas hannai*	*Lamprocyrtis nigriniae*	*Theocorythium trachelium trachelium*	*Axoprunum angelinum*	*Didymocyrtis tetrathalamus tetrathalamus*	*Eucyrtidium calvertense*	*Eucyrtidium teuscheri teuscheri*	*Pterocanium praetextum eucolpum*	*Pterocanium trilobum*	*Saturnalis circularis*	*Spongaster tetras tetras*	*Lamprocyrtis heteroporos*	*Lamprocyrtis neoheteroporos*	*Amphirhopalum ypsilon*
		175-1080A-																				
Quaternary	*B. invaginata–C. tuberosa*	1H-CC	3.25	C	G	+	P	+	P	+	P											
Pleistocene	*A. angelinum–A. ypsilon*	2H-CC	13.15	C	G		P	+	P			P	P	+	+	P	+	+				
Pleistocene	*A. angelinum–A. ypsilon*	3H-CC	23.13	F	G		P		+			P	+					+	+			
Pleistocene	*A. angelinum–A. ypsilon*	4H-CC	34.07	C	G		P	+	P			P	P	P	+	P		P				
Pleistocene	*A. angulare*?	5H-CC	42.50	A	G		P	+	P			P	P	P	+	P	P	+		P	P	
Pleistocene	*A. angulare*?	6H-CC	51.27	C	G		P		P			P	P	P			P	P		+	P	P

Notes: Occurrence is indicated by P = present and + = one specimen per slide. Abundance: C = common; F = few; and A = abundant. Preservation: G = good. *B. invaginata = Bucciuosphaera invaginata; C. tuberosa = Collosphaera tuberosa; A. angelinum = Axoprunum angelinum; A. ypsilon = Amphirhopalum ypsilon; A. angulare = Authocyrtidium angulare.*

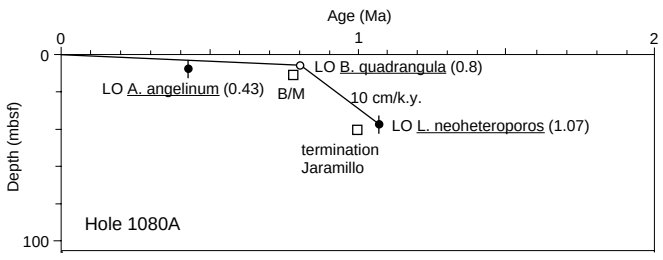

Figure 8. Age-depth plot and sedimentation rates estimated from silicoflagellate (open circle) and radiolarian (solid circles) datums at Hole 1080A. Open squares = magnetic polarity boundaries.

presence of a significant secondary magnetization. The intensity of NRM after 20-mT demagnetization is similar in magnitude at both holes, ranging generally from ~10^{-4} to ~10^{-3} A/m (Fig. 10, left panel). The intensity decreases sharply at the polarity boundaries identified at both holes. Below ~40 m at Hole 1080A, the intensity decreases from ~10^{-4} A/m to ~10^{-5}, where magnetic susceptibility also shows some decrease.

Magnetostratigraphy

We identified the polarity of the NRM from the declinations and inclinations (Fig. 10, middle and right panels). Based on the biostratigraphy (see “Biostratigraphy and Sedimentation Rates” section,

this chapter), the upper normal-polarity zone (above 9.5 mbsf at Hole 1080A and above 9 mbsf at Hole 1080B) is identified as the Brunhes Chron (C1n, 0.78 Ma; Berggren et al., 1995), the reversed-polarity zone as the Matuyama Chron, and the lower normal-polarity zone between 41 and 51 mbsf at Hole 1080B as the Jaramillo Subchron (C1r.1n, 0.99–1.07 Ma; Berggren et al., 1995). The Jaramillo Subchron was not observed at Hole 1080B, but the intensity decrease at the bottom of the hole suggests that the termination of the Jaramillo Subchron may occur just below the bottom of the hole. The fluctuation of directions and very low intensities from ~12 mbsf at Hole 1080A is interpreted as the onset of the Brunhes/Matuyama transition. At ~9.8 mbsf, the transition record abruptly terminates, which coincides with the presence of silty bands in the sediment. The biostratigraphy suggests the presence of a hiatus at the silty bands. At Hole 1080B, the polarity boundary occurs within a gap between Cores 175-1080B-1H and 2H; the transitional record was not observed.

The average sedimentation rate between the Brunhes/Matuyama boundary and the termination of the Jaramillo Subchron is ~150 m/m.y. The high sedimentation rate at this site in the late Matuyama Chron and the NRM with little magnetic overprint could give us a rare opportunity to study detailed magnetic field behavior during this period of time. A steep decrease in the remanent intensity with a fluctuation of direction occurs at 26 mbsf at Hole 1080A and at 24 mbsf at Hole 1080B. This does not coincide with a low in magnetic susceptibility, which occurs ~0.5 m shallower than the intensity low. This is probably a short normal-polarity event or excursion in the late Matuyama Chron, possibly the Kamikatsura event (0.85 Ma; Harland et al., 1990).

COMPOSITE SECTION

Holes 1080A and 1080B were cored with the APC to a maximum depth of 50.3 mbsf at Site 1080. Measurements of magnetic susceptibility and GRAPE density were made on the MST, and color reflectance was measured with the Minolta spectrophotometer. All parameters were measured at 2-cm resolution at Hole 1080A and at 4-cm resolution at Hole 1080B. Graphic and quantitative alignment of stratigraphic features of the MST and color reflectance data were used to depth adjust adjacent cores to establish a meters composite depth (mcd) scale. Beginning from the core top, a constant is added to the mbsf scale to establish depth offsets for each core to assemble a single continuous composite section. For Site 1080, continuity of the composite section was documented to 44 mcd.

Construction of the composite section and determination of core gaps were constrained primarily by the magnetic susceptibility and, to a lesser extent, by using GRAPE density data. Color reflectance parameters chromaticity (b*), red/blue ratio [650 nm/450 nm], and lightness (L*) were used in support of the MST data. Data were filtered because gas voids and core expansion induced considerable noise into the physical properties measurements. Details of the filtering process are documented in the "Composite Section" section of the "Site 1075" chapter (this volume), with the exception that a seven-point Gaussian filter was used to smooth the color reflectance data, and a six-point Gaussian filter was applied to the GRAPE measurements.

The composite depth section shows excellent agreement between Holes 1080A and 1080B (Fig. 11). Depth offsets for individual cores relative to their meters below seafloor positions are given in Table 5. Intracore stretching and compression often lead to feature mismatches of the data, which are indicative of core distortion and cannot be resolved with a single depth adjustment per core. The splice at 34 mcd is based upon magnetic susceptibility; however, it is weakly supported by the other parameters and should be regarded with caution. Core expansion relative to the mbsf scale is ~8% (Fig. 12).

Table 4. Tensor tool–orientation data for cores from Holes 1080A and 1080B.

Core	MTF (°)	Inclination angle
175-1080A-		
4H	223	1.15
5H	86	1.25
6H	220	1.29
175-1080B-		
3H	273	0.63
4H	274	0.33

Notes: The orientation parameter (MTF) is the angle in degrees between magnetic north and the double line marked on the center of the working half of the core. The local declination anomaly is 12°W.

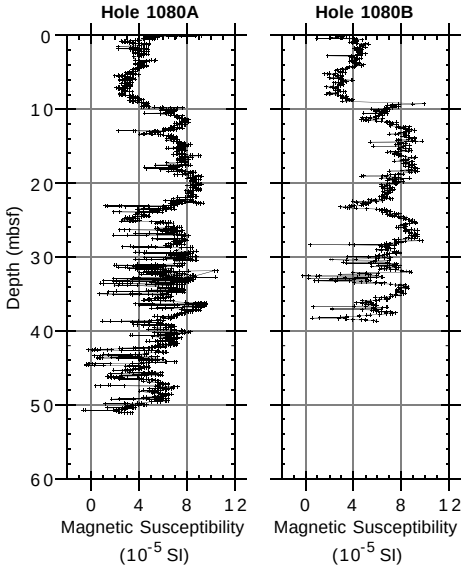

Figure 9. Magnetic susceptibility from MST data (volume corrected) for Holes 1080A and 1080B.

From the composite record, a continuous spliced record for Site 1080 was established using the aligned cores of Holes 1080A and 1080B (Fig. 13). The Site 1080 splice can be used as a sampling guide to recover a single sedimentary sequence from the top 44 mcd (42 mbsf). Tie points for the Site 1080 splice are given in Table 6.

INORGANIC GEOCHEMISTRY

Thirty-one interstitial water samples were gathered from Hole 1080A over a depth range from 1.4 to 49.64 mbsf (Table 7), at a typical high-resolution frequency of one sample per section of core. Termination of drilling was caused by the presence of a dolomite layer at ~50 mbsf, and the high-resolution interstitial water program fortuitously was able to focus in detail on dolomitization processes operating throughout the recovered sequence. The chemical processes involved in organic carbon degradation and carbonate dissolution and reprecipitation dominate the interstitial water chemical distributions at Site 1080.

Alkalinity, Sulfate, and Ammonium

Downcore profiles of alkalinity, sulfate, and ammonium at Site 1080 (Fig. 14) record the degradation of organic matter. Sulfate is es-

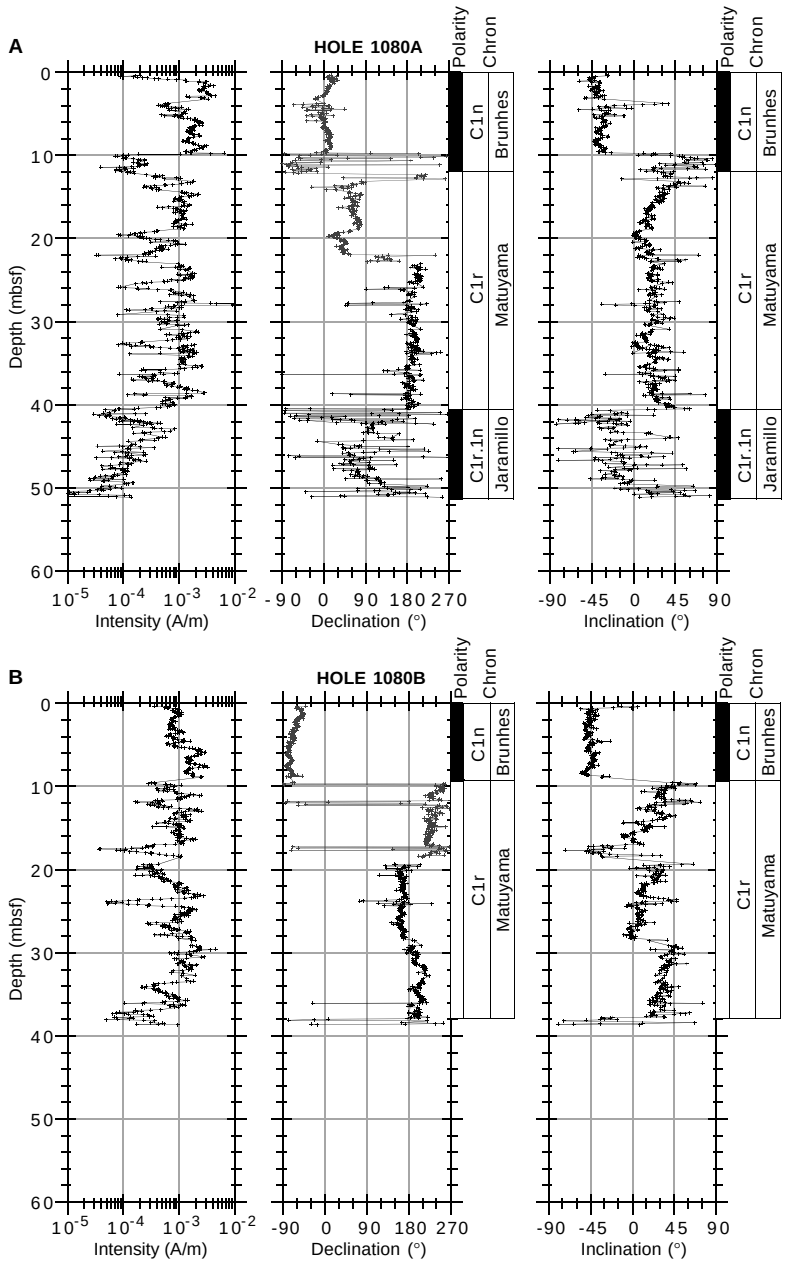

Figure 10. NRM intensity, declination, inclination, and magnetostratigraphic interpretation after 20-mT demagnetization for (**A**) Hole 1080A and (**B**) Hole 1080B. Black symbols = Tensor corrected; gray symbols = uncorrected. Polarity shading: black = normal and white = reversed.

sentially completely consumed within the upper 10 mbsf. Alkalinity values increase dramatically through this uppermost depth interval, and the concentration of ammonium also shows the greatest increase. From 10 mbsf to the dolomite layer at 50 mbsf, alkalinity and ammonium both increase monotonically.

Calcium, Magnesium, and Strontium

Concentration profiles of Ca^{2+}, Mg^{2+}, and Sr^{2+} reflect processes of carbonate dissolution and precipitation (Fig. 15). The upper 10 mbsf at Site 1080 is characterized by sharply decreasing concentrations of sedimentary calcium carbonate, with values changing from ~26 to <5 wt% through this depth range (see "Organic Geochemistry" section, this chapter). Concentrations of dissolved Sr^{2+} increase through this interval, indicating dissolution of sedimentary calcite. In addition to the Sr^{2+} distributions, the one-point maximum in both Ca^{2+} and Mg^{2+} concentrations at 2.9 mbsf may also be recording this dissolution.

Both Ca^{2+} and Mg^{2+} concentrations systematically decrease with depth down to ~25 mbsf. We interpret these decreases as recording carbonate precipitation including dolomitization; in the upper 25 mbsf, the decrease in Ca^{2+} (7 mM) almost matches the associated decrease in Mg^{2+} (10 mM). An unknown portion of the Mg^{2+} depletion is accounted for by uptake by clay minerals. From 25 mbsf to the dolomite layer at 50 mbsf, both Ca^{2+} and Mg^{2+} remain essentially constant. Through the entire 50-m depth cored here, the overall decrease in Mg^{2+} describes a gradient of 0.18 mM Mg^{2+} per meter of sediment, which is the largest gradient observed so far during Leg 175. Gradients of the decrease in Mg^{2+} concentration at Sites 1075, 1076, 1077, 1078, and 1079 range between 0.06 mM/m and 0.12 mM/m. Although the formation of disseminated dolomite is occurring at these other sites, the presence of the completely lithified dolomite layer at

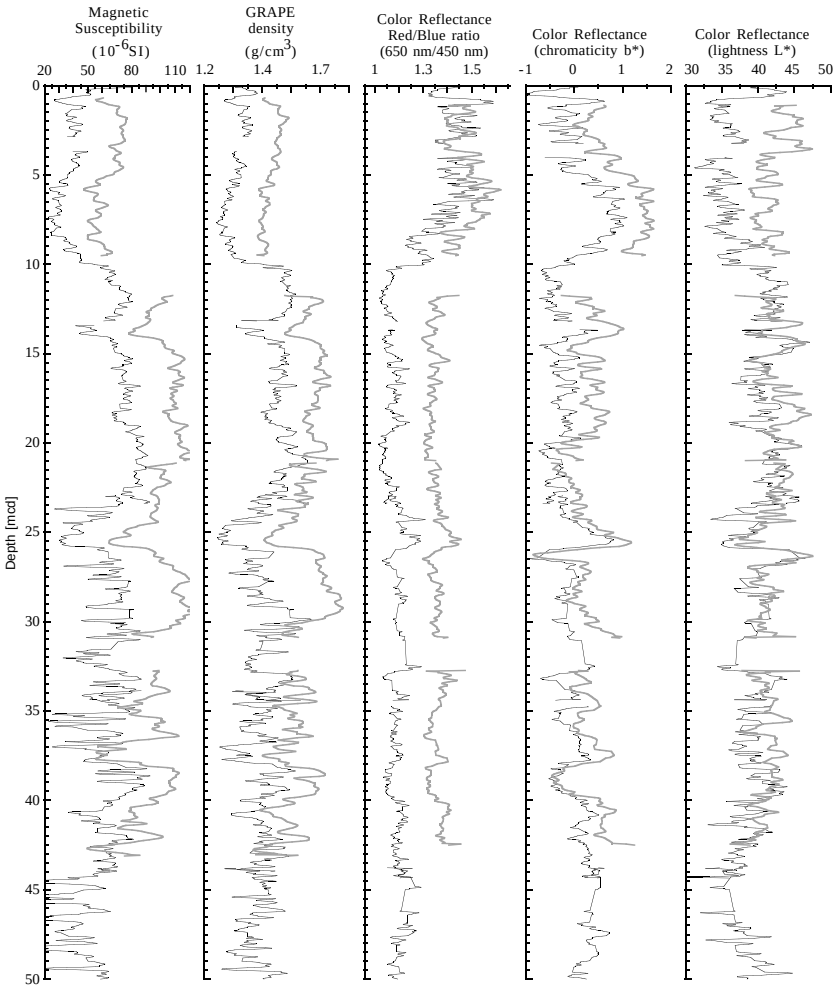

Figure 11. Composite section for Site 1080. Magnetic susceptibility, GRAPE bulk density, and the color reflectance (chromaticity b*, red/blue ratio [650 nm/450 nm], and lightness L*) data are plotted for Holes 1080A (black line) and 1080B (gray line). The downhole logs are shown in meters composite depth (mcd). An offset 1.5 times the standard deviation of the Hole 1080A data has been applied to Hole 1080B for clarity in viewing the composite sections.

Table 5. Offsets applied to cores from Holes 1080A and 1080B.

Core	Depth (mbsf)	Offset (m)	Composite depth (mcd)
175-1080A-			
1H	0.0	0.00	0.00
2H	3.3	0.31	3.61
3H	12.8	0.55	13.35
4H	22.3	0.58	22.88
5H	31.8	2.00	33.80
6H	41.3	2.00	43.30
175-1080B-			
1H	0.0	0.62	0.62
2H	9.2	2.47	11.67
3H	18.7	2.34	21.04
4H	28.2	4.45	32.65

Note: The offsets transform ODP standard depth values in meters below seafloor (mbsf) to meters composite depth (mcd).

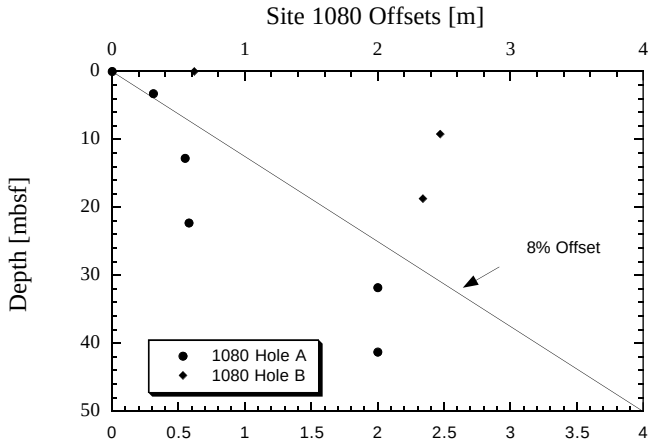

Figure 12. Core offsets applied to Site 1080 plotted against standard ODP meters below seafloor (mbsf). A linear 8% growth of meters composite depth (mcd) compared with mbsf is indicated by a line.

50 mbsf at Site 1080 suggests that dolomitization is of greater importance at Site 1080 than has been observed at previous Leg 175 sites.

These preliminary data also suggest that the dolomite layer responsible for terminating drilling is, in fact, a relict dolomite layer. Were the layer actively growing at the present time, the depletion gradients of Ca^{2+} and Mg^{2+} would record continual depletion toward the layer itself, rather than recording no change in either Ca^{2+} or Mg^{2+} from 25 mbsf to that horizon.

Silica and Phosphate

Dissolved silica increases in concentration very rapidly from representative bottom-water values through the uppermost 4 m of sedi-

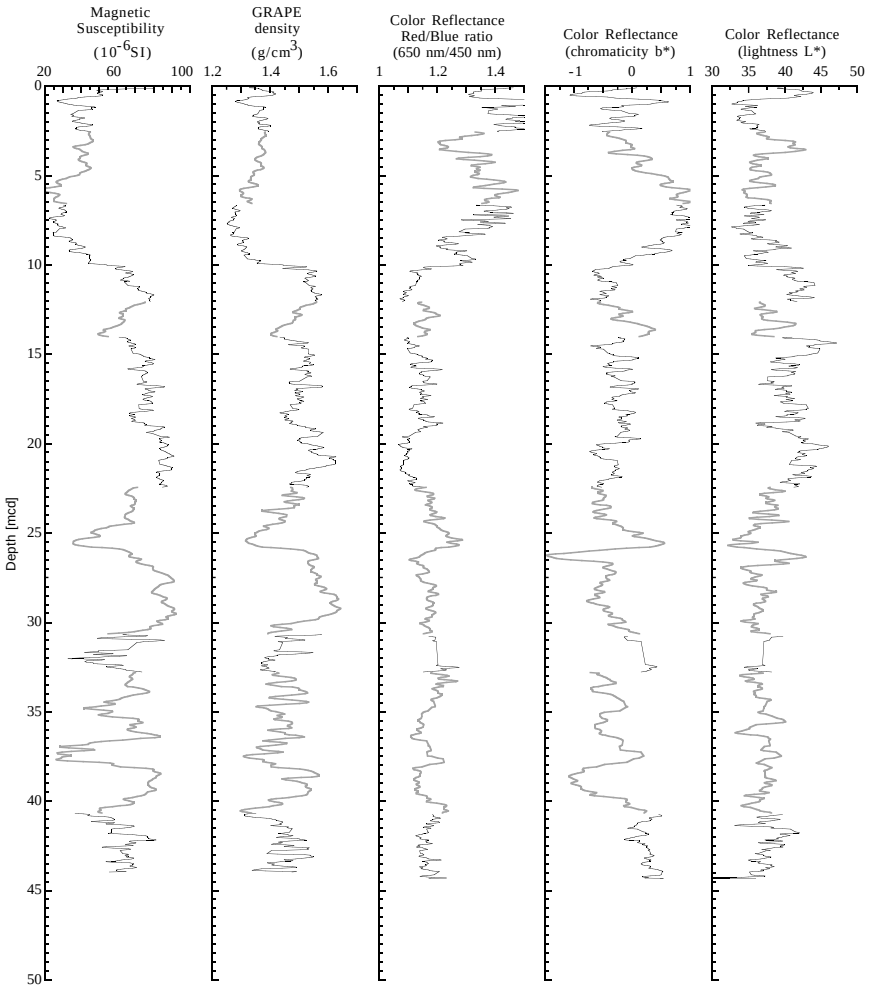

Figure 13. Spliced records for magnetic susceptibility, GRAPE bulk density, and color reflectance (chromaticity b*, red/blue ratio [650 nm/450 nm], and lightness L*) plotted in meters composite depth (mcd). Cores from two holes at Site 1080 have been used for the spliced record: black line = Hole 1080A and gray line = Hole 1080B.

Table 6. List of splice tie points used to create the continuous "spliced" stratigraphic sequence for Site 1080.

Hole, core, section, interval (cm)	Depth (mbsf)	Composite depth (mcd)	Whether tied	Hole, core, section, interval (cm)	Depth (mbsf)	Composite depth (mcd)
1080A-1H-2, 104	2.54	2.54	Tie to	1080B-1H-2, 41	1.92	2.54
1080B-1H-4, 144	5.94	6.56	Tie to	1080A-2H-2, 145	6.25	6.56
1080A-2H-6, 92	11.72	12.03	Tie to	1080B-2H-1, 36	9.56	12.03
1080B-2H-2, 84	11.54	14.01	Tie to	1080A-3H-1, 66	13.46	14.01
1080A-3H-6, 132	21.87	22.42	Tie to	1080B-3H-1, 137	20.08	22.42
1080B-3H-7, 60	28.30	30.64	Tie to	1080A-4H-9, 83	30.06	30.64
1080A-4H-1, 128	32.19	32.77	Tie to	1080B-4H-1, 12	28.32	32.77
1080B-4H-6, 112	36.22	40.67	Tie to	1080A-5H-7, 12.5	38.67	40.67
1080A-5H-1, 24	42.34	44.34				

Note: The tie points are listed in standard ODP meters below seafloor (mbsf) and meters composite depth (mcd).

ment (Fig. 16), recording the dissolution of biogenic opal. Below ~10 mbsf, the concentration of dissolved silica remains essentially constant to the bottom of the hole.

Dissolved phosphate increases from values representative of bottom water to a maximum of ~180 µM within the uppermost 10 mbsf. Phosphate concentrations below this depth increase only slightly to a maximum of 190 µM at 32 mbsf before decreasing to ~130 µM at the dolomite layer. The decrease in dissolved phosphate most likely records uptake by diagenetic apatite.

Sodium and Potassium

Concentrations of dissolved Na^+ and K^+ decrease through the uppermost 4 to 8 mbsf, below which concentrations of Na^+ gradually increase with depth, whereas K^+ remains essentially constant (Fig. 17). These variations are most likely reflecting uptake and release by clay minerals.

Salinity and Chloride

Salinity decreases smoothly downcore (Fig. 18), most likely reflecting the decreases of Mg^{2+} and Ca^{2+} described previously. Dissolved Cl^- records an initial increase to 8 mbsf, as has been observed at previous Leg 175 sites (and which we attribute to variability in the glacial ocean), followed by a continual decrease to the dolomite layer at 50 mbsf.

ORGANIC GEOCHEMISTRY

Calcium carbonate and organic carbon concentrations were measured on sediment samples from Site 1080 (Table 8). Organic matter atomic carbon/nitrogen (C/N) ratios and Rock-Eval analyses were employed to determine the type of organic matter contained within

Table 7. Interstitial water composition for Hole 1080A.

Core, section, interval (cm)	Depth (mbsf)	pH	Alkalinity (mM)	Salinity	Cl^- (titr) (mM)	Cl^- (IC) (mM)	SO_4^{2-} (mM)	Na^+ (mM)	Mg^{2+} (mM)	Ca^{2+} (mM)	K^+ (mM)	H_4SiO_4 (µM)	NH_4^+ (µM)	PO_4^{3-} (µM)	Sr^{2+} (µM)
175-1080A-															
1H-1, 140-150	1.40	7.72	5.381	35.5	555	552	26.17	484	49.91	8.80	11.68	659	434	19	91
1H-2, 140-150	2.90	8.05	9.840	35.0	557	552	23.74	480	51.95	9.70	11.26	724	1,007	46	92
2H-1, 140-150	4.70	8.21	34.729	35.0	559	549	4.66	481	49.26	6.41	10.84	776	2,877	150	97
2H-2, 140-150	6.20	8.20	38.841	35.0	560	555	0.73	484	48.00	4.84	10.72	759	3,446	167	100
2H-3, 140-150	7.70	8.12	37.650	35.0	565	554	1.76	490	48.41	4.39	10.90	743	4,906	178	102
2H-4, 140-150	9.20	8.48	41.086	34.5	565	556	0.29	491	47.87	4.33	11.28	812	4,588	174	105
2H-5, 140-150	10.70	8.37	39.443	34.5	564	556	0.21	489	47.11	4.63	11.39	881	4,664	161	106
2H-6, 140-150	12.20	7.83	37.338	34.5	561	555	0.34	487	46.21	3.63	12.34	793	4,895	168	103
3H-1, 140-155	14.20	7.64	38.960	34.5	563	556	0.12	489	46.64	4.00	11.52	833	5,849	144	104
3H-2, 140-155	15.75	7.62	35.363	34.5	564	559	0.53	489	45.92	4.12	11.38	731	6,254	159	102
3H-3, 140-155	17.30	7.86	40.143	34.5	560	556	1.09	493	45.16	3.85	11.45	752	7,186	170	102
3H-4, 140-155	18.85	7.93	39.377	34.5	560	552	0.00	491	44.71	3.54	11.57	826	6,232	182	101
3H-5, 140-155	20.40	8.25	39.493	34.5	558	554	0.43	491	44.02	4.15	11.14	814	6,682	188	98
3H-6, 140-155	21.95	7.95	40.093	34.5	558	557	0.17	493	43.50	3.65	11.09	666	6,868	190	97
4H-2, 140-150	24.04	7.59	38.742	34.5	557	555	0.11	493	43.14	3.21	10.95	764	7,384	191	101
4H-3, 140-150	25.54	7.63	36.754	34.0	557	554	0.08	496	40.38	2.23	13.06	633	8,338	167	85
4H-5, 140-150	27.20	8.43	39.903	34.0	557	555	0.70	499	40.10	2.75	13.98	600	9,818	182	96
4H-7, 140-150	28.81	7.94	39.147	34.0	557	557	0.00	498	39.97	2.63	13.00	640	8,985	184	97
4H-9, 145-155	30.61	8.43	41.288	34.0	557	556	0.00	499	40.85	3.16	10.94	836	8,425	187	104
4H-11, 140-150	32.31	7.96	38.843	34.0	552	560	0.00	495	38.82	2.75	12.70	669	5,432	190	99
5H-2, 120-130	33.92	7.84	41.202	34.0	556	554	0.74	504	39.49	2.67	11.23	700	9,752	136	104
5H-4, 77-87	36.00	8.11	41.651	34.0	540	537	0.00	489	38.63	2.36	11.01	705	11,145	125	101
5H-6, 110-120	38.40	7.50	43.418	34.0	558	559	0.00	504	40.60	2.83	10.45	762	11,013	153	106
5H-7, 110-120	39.60	7.78	43.907	34.0	555	557	0.00	503	40.26	2.53	11.07	795	10,553	145	103
5H-8, 110-120	40.80	7.48	43.509	34.0	547	547	0.07	496	39.21	2.57	11.53	716	11,211	130	103
5H-9, 110-120	42.00	8.14	39.942	34.0	557	553	0.00	504	38.21	2.57	12.22	664	13,042	100	101
6H-2, 130-140	43.04	7.66	44.055	34.0	554	558	0.84	504	39.96	2.47	11.19	762	11,868	119	104
6H-4, 130-140	45.44	7.37	46.953	34.0	552	556	0.38	503	40.25	2.68	10.33	805	10,838	153	107
6H-5, 130-140	46.84	7.80	44.986	34.0	535	553	0.47	490	37.55	2.37	11.30	728	11,265	107	101
6H-6, 130-140	48.24	7.35	47.380	34.0	554	548	0.28	505	40.78	2.62	11.00	795	11,309	141	97
6H-7, 130-140	49.64	7.17	47.703	34.0	551	548	0.55	504	40.03	2.39	10.80	774	11,748	128	105

Note: Cl^- (titr) = analyzed by titration and Cl^- (IC) = analyzed by ion chromatography.

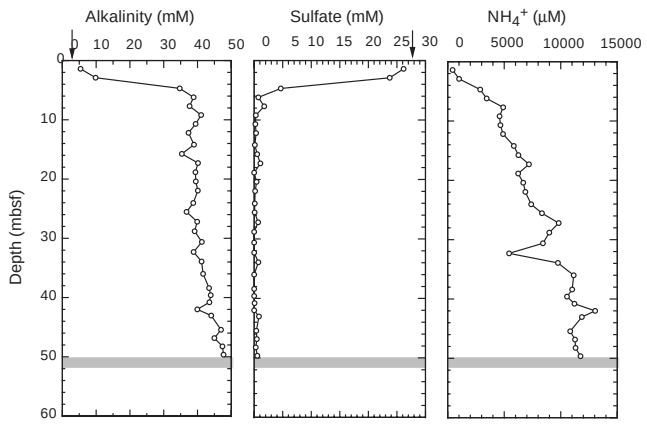

Figure 14. Downcore profiles of dissolved alkalinity, sulfate, and ammonium at Site 1080. Arrows = mean ocean-bottom-water values taken from Millero and Sohn (1992). Shaded region = position of dolomite layer; no particular layer thickness is implied.

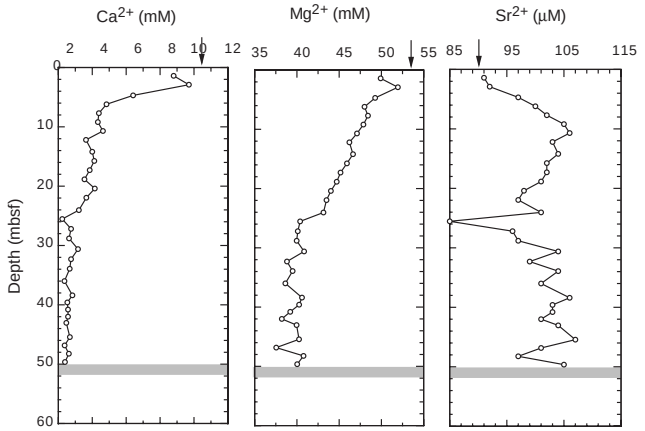

Figure 15. Downcore profiles of Ca^{2+}, Mg^{2+}, and Sr^{2+} at Site 1080. Arrows = mean ocean-bottom-water values taken from Millero and Sohn (1992). Shaded region = position of dolomite layer; no particular layer thickness is implied.

the sediments. High gas contents were encountered, and routine monitoring of the sedimentary gases was done for drilling safety.

Inorganic and Organic Carbon Concentrations

Concentrations of carbonate carbon are low in most Site 1080 sediments. Sample 175-1080A-1H-1, 46–47 cm, contains 3.1 wt% inorganic carbon, but concentrations quickly decrease with depth (Table 8). The maximum carbonate carbon concentration is equivalent to 26.1 wt% sedimentary $CaCO_3$. These moderately low concentrations agree with the low abundances of coccoliths and foraminifer microfossils in these hemipelagic sediments (see "Biostratigraphy and Sedimentation Rates" section, this chapter). The decrease in carbonate concentrations is probably largely a result of dissolution fueled by oxidation of organic matter (see "Inorganic Geochemistry" section, this chapter).

TOC values range from 3.86 to 1.10 wt% (Table 8) and average 2.40 wt%. The concentrations are nearly 10 times greater than the average of 0.3 wt% given by McIver (1975) based on DSDP Legs 1–33, a value that can be considered representative of typical deep-sea sediments. The high TOC concentrations at this site may be ascribed to a combination of a high supply of organic matter from elevated paleoproductivities and a high accumulation rate of sediments, enhancing the preservation of organic matter.

Organic Matter Source Characterization

Organic C/N ratios were calculated for Site 1080 samples using TOC and total nitrogen concentrations to help identify the origin of their organic matter. Site 1080 C/N ratios vary from 14.2 to 8.4 (Table 8). The C/N ratios average 11.1, a value that is intermediate between unaltered algal organic matter (5–8) and fresh land-plant

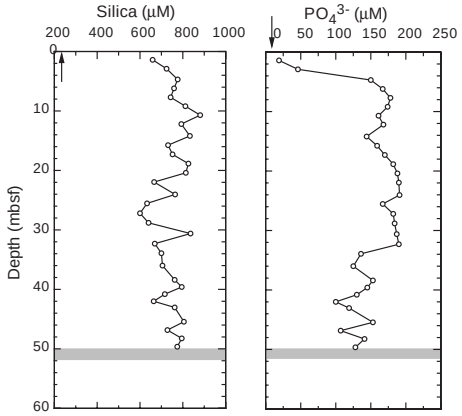

Figure 16. Downcore profiles of dissolved silica and phosphate at Site 1080. Arrows = mean ocean-bottom-water values taken from Millero and Sohn (1992). Shaded region = position of dolomite layer; no particular layer thickness is implied.

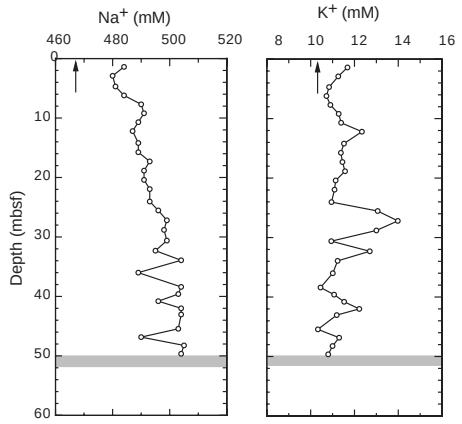

Figure 17. Downcore profiles of dissolved Na^+ and K^+ at Site 1080. Arrows = mean ocean-bottom-water values taken from Millero and Sohn (1992). Shaded region = position of dolomite layer; no particular layer thickness is implied.

material (25–35; e.g., Emerson and Hedges, 1988; Meyers, 1994). It is probable that these organic carbon–rich sediments contain a mixture that is made up mostly of degraded algal material and partly of detrital continental organic matter. The C/N ratios that are higher than fresh algal organic matter indicate that preferential loss of nitrogen-rich, proteinacous matter and consequent elevation of C/N ratios occurred during settling of organic matter to the seafloor. Such early diagenetic alteration of C/N ratios is often seen under areas of elevated marine productivity, such as the Angola margin (Meyers, 1997).

A Van Krevelen–type plot of hydrogen index (HI) and oxygen index (OI) values (Fig. 19) similarly indicates that the sediments contain type II (algal) organic matter that has been altered by microbial processing during early diagenesis. Well-preserved type II organic matter has high HI values (Peters, 1986), which can be lowered by microbial oxidation (Meyers, 1997). The low HI values of fresh type III organic matter, however, cannot become elevated by postdepositional alteration. Site 1080 sediments having higher Rock-Eval TOC values also have higher HI values (Fig. 20). This relationship confirms that the algal organic matter has been partially oxidized. Further evidence of substantial amounts of in situ organic matter degradation exists in the large decreases in sulfate and increases in alkalinity in the interstitial waters of Site 1080 sediments (see "Inorganic Geochemistry" section, this chapter).

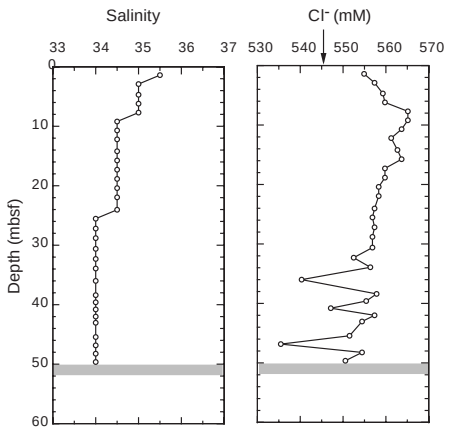

Figure 18. Downcore profiles of salinity and dissolved Cl^- at Site 1080. Arrow = mean ocean-bottom-water value taken from Millero and Sohn (1992). Shaded region = position of dolomite layer; no particular layer thickness is implied.

Rock-Eval T_{max} values are low (Table 9), showing that organic matter is thermally immature with respect to petroleum generation (Peters, 1986). The low thermal maturity is consistent with the measured geothermal gradient of 45.7°C/km at this site (see "Physical Properties" section, this chapter).

Headspace Gases

Sediments from Site 1080 had high gas content. Gas pressures became great enough in sediments below the first core to require perforating the core liner to relieve the pressure and minimize core expansion. Natural gas analyses determined that most of this gas was CO_2, and headspace concentrations of this gas continued to increase to the bottom of Hole 1080A (50 mbsf; Fig. 19). Hydrogen sulfide could be detected at a concentration of 4 ppm in Core 175-1080A-1H. A moderate to weak odor of H_2S prevailed from near-surface sediments through Core 175-1080A-3H (22 mbsf).

Methane (C_1) first appears in significant concentrations in headspace gas samples at 6.3 mbsf. Concentrations rapidly increase and are high in sediments below 7 mbsf (Fig. 20). As at Site 1075 and the other sites off Angola, high methane/ethane (C_1/C_2) ratios and the absence of major contributions of higher molecular weight hydrocarbon gases (Table 10) indicate that the gas is biogenic, as opposed to thermogenic, in origin. A biogenic origin of the methane is supported by the disappearance of interstitial sulfate at approximately the same sub-bottom depth where methane concentrations begin to rise (see "Inorganic Geochemistry" section, this chapter). As noted by Claypool and Kvenvolden (1983), the presence of interstitial sulfate inhibits methanogenesis in marine sediments.

PHYSICAL PROPERTIES

Near continuous density, magnetic susceptibility, and natural gamma radiation measurements were carried out with the MST on whole-round sections of cores from each hole (see "Explanatory Notes" chapter, this volume). Results from compressional (*P*-wave) ultrasonic velocity measurements with the MST were disregarded because of very high noise level (see "Physical Properties" section, "Site 1076" chapter, this volume).

Table 8. Percentages of inorganic and total carbon, total nitrogen, and total sulfur in sediment samples from Hole 1080A.

Core, section, interval (cm)	Depth (mbsf)	IC (wt%)	$CaCO_3$ (wt%)	TC (wt%)	TOC (wt%)	TN (wt%)	TS (wt%)	C/N (atomic)
175-1080A-								
1H-1, 46-47	0.46	3.14	26.1	4.24	1.10	0.15	0.20	8.6
1H-2, 46-47	1.96	1.69	14.1	4.27	2.58	0.31	1.00	9.8
2H-1, 46-47	3.76	1.22	10.2	4.06	2.84	0.31	1.26	10.6
2H-3, 46-47	6.76	1.15	9.6	4.76	3.61	0.37	1.28	11.5
2H-5, 46-47	9.76	0.76	6.4	2.45	1.69	0.19	1.09	10.5
3H-1, 46-47	13.26	0.20	1.6	3.28	3.08	0.29	2.27	12.4
3H-3, 46-47	16.36	0.27	2.2	2.61	2.34	0.24	1.93	11.6
3H-5, 46-47	19.46	0.74	6.2	2.57	1.83	0.20	0.83	10.9
4H-2, 45-47	23.09	0.25	2.1	2.56	2.31	0.22	1.19	12.1
4H-3, 46-47	24.60	0.20	1.7	3.19	2.99	0.26	1.96	13.3
4H-7, 50-51	27.91	0.84	7.0	2.93	2.09	0.22	1.28	11.3
5H-1, 46-47	32.26	0.34	2.8	2.24	1.90	0.22	1.84	10.2
5H-3, 46-47	34.48	0.29	2.4	2.79	2.49	0.26	1.40	11.4
5H-5, 46-47	36.56	0.80	6.6	2.22	1.43	0.20	1.16	8.4
5H-9, 46-47	41.36	0.18	1.5	2.51	2.32	0.25	1.77	10.9
6H-3, 42-43	43.56	0.21	1.8	4.07	3.86	0.32	1.54	14.2

Notes: IC = inorganic carbon; $CaCO_3$ = calcium carbonate; TC = total carbon; TOC = total organic carbon; TN = total nitrogen; TS = total sulfur; and C/N = carbon/nitrogen ratio. TOC concentrations are calculated from the difference between IC and TC concentrations. C/N ratios are calculated from TOC and TN concentrations and are given as atom/atom ratios.

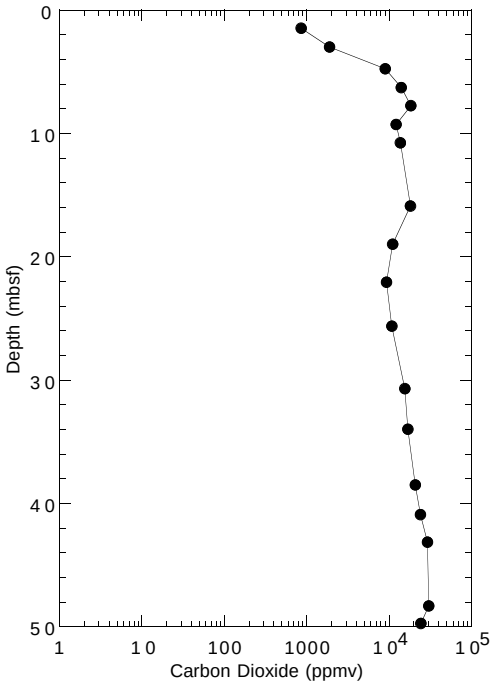

Figure 19. Headspace CO_2 concentrations in sediments from Hole 1080A.

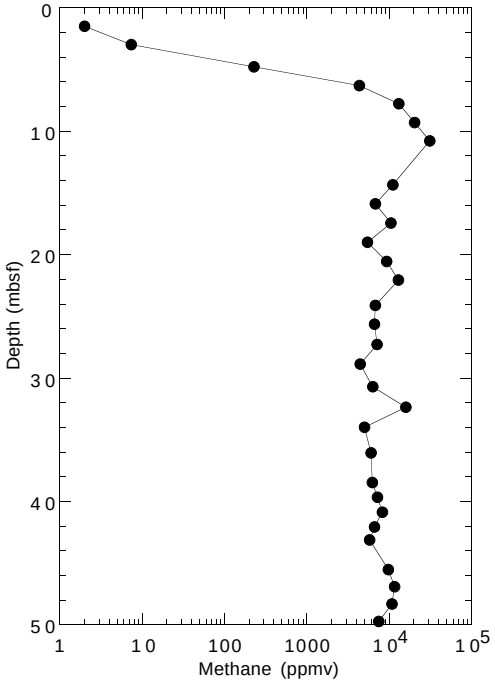

Figure 20. Headspace methane concentrations in sediments from Hole 1080A.

Index properties (gravimetric density, porosity, and moisture content) were measured on one or two samples (volume = ~10 cm^3) per working-half section on all cores from Hole 1080A, using Method C (see "Explanatory Notes" chapter, this volume).

Discrete ultrasonic compressional (*P*-wave) velocities and undrained vane-shear measurements were conducted at a resolution of one or two samples per section close to the index properties samples. The modified Hamilton Frame was used for the discrete *P*-wave measurements.

Multisensor Track

The sampling interval for GRAPE density (Fig. 21) and magnetic susceptibility measurements (Fig. 22A) was 2 cm for the recovered core depth of 52 mbsf. MST data are included on CD-ROM (back pocket, this volume). Natural gamma radiation was measured with a sampling period of 30 s at 32-cm resolution (Fig. 22B). Profiles of magnetic susceptibility and natural gamma radiation correspond very well to each other (Figs. 22A and B, respectively). The correlation between GRAPE density and discrete wet bulk density data is good (Fig. 21), with slightly higher GRAPE values between 0 and 22 mbsf, and lower values below 25 mbsf. A sharp increase in density occurs at 10 mbsf.

Velocities

The near-continuous velocity profile recorded with the MST was disregarded because of instrumental problems and high scatter caused by limited core quality. Discrete velocity values vary over a narrow range between 1540 and 1570 m/s (Fig. 23). Some similari-

Table 9. Results of Rock-Eval pyrolysis analyses of sediments from Hole 1080A.

Core, section, interval (cm)	Depth (mbsf)	TOC (wt%)	S_1	S_2	S_3	T_{max} (°C)	HI	OI
175-1080A-								
1H-2, 46-47	1.96	2.58	1.00	6.45	4.54	414	250	175
4H-3, 46-47	24.60	2.99	1.40	10.79	2.13	397	360	71
5H-5, 46-47	36.56	1.43	0.81	3.55	3.13	398	248	218
6H-3, 42-43	43.56	3.86	1.79	13.97	2.73	401	361	70

Notes: TOC = total organic carbon; HI = hydrogen index; and OI = oxygen index. Units of the various Rock-Eval parameters are given in the "Organic Geochemistry" section of the "Explanatory Notes" chapter (this volume).

Table 10. Results of headspace gas analyses of sediments from Hole 1080A.

Core, section, interval (cm)	Depth (mbsf)	C_1 (ppmv)	CO_2 (ppmv)	C_2= (ppmv)	C_2 (ppmv)	C_3 (ppmv)	C_1/C_2
175-1080A-							
1H-2, 0-5	1.50	2	864				
1H-3, 0-5	3.00	7.4	1,893				
2H-2, 0-5	4.80	228	9,058	0.2	2.1		109
2H-3, 0-5	6.30	4,352	14,123	0.3	4.5		967
2H-4, 0-5	7.80	13,099	18,397	0.6	7.2	0.8	1,819
2H-5, 0-5	9.30	20,309	12,152	0.7	8.5	1.2	2,389
2H-6, 0-5	10.80	31,121	13,778	0.2	10.9	1.3	2,855
3H-2, 0-5	14.35	11,025		1.0	6.0	1.5	1,838
3H-3, 0-5	15.90	6,842	18,213	1.7	6.8	3.0	1,006
3H-4, 0-5	17.45	10,556		0.3	6.8	2.1	1,552
3H-5, 0-5	19.00	5,485	11,171	0.5	4.1	1.1	1,338
3H-6, 0-5	20.55	9,351		0.3	6.0	1.8	1,558
3H-7, 0-5	22.10	12,959	9,367	0.4	8.2	2.5	1,580
4H-3, 0-5	24.14	6,827		0.3	5.0	1.9	1,365
4H-4, 0-5	25.64	6,684	10,766	0.4	3.6	1.0	1,857
4H-6, 0-5	27.30	7,158		0.5	6.0	2.3	1,193
4H-8, 0-5	28.91	4,458		1.4	5.1	2.6	874
4H-10, 0-5	30.71	6,333	15,641	0.9	7.1	3.7	892
4H-12, 0-5	32.41	16,069		0.8	10.9	3.7	1,474
5H-3, 0-5	34.02	4,999	16,914	1.2	4.8	2.6	1,041
5H-5, 0-5	36.10	6,021		1.2	3.9	3.0	1,544
5H-7, 0-5	38.50	6,220	20,790	1.3	3.6	3.1	1,728
5H-8, 0-5	39.70	7,196		1.8	4.6	4.1	1,564
5H-9, 0-5	40.90	8,257	24,275	1.1	3.6	3.3	2,294
5H-10, 0-5	42.10	6,611		0.1	4.4	2.9	1,502
6H-3, 0-5	43.14	5,787	29,362	1.1	5.0	6.9	1,157
6H-5, 0-5	45.54	9,881		1.1	6.4	7.0	1,544
6H-6, 0-5	46.94	11,664		1.4	16.1	4.5	7,24
6H-7, 0-5	48.34	10,759	30,280	1.0	6.4	5.7	1,681
6H-8, 0-5	49.74	7,458	24,423	0.2	3.5	3.0	2,131

Notes: C_1 = methane; CO_2 = carbon dioxide; C_2= = ethene; C_2 = ethane; and C_3 = propane. Dominance of C_1 over C_2 indicates that the gases originate from in situ microbial degradation of organic matter.

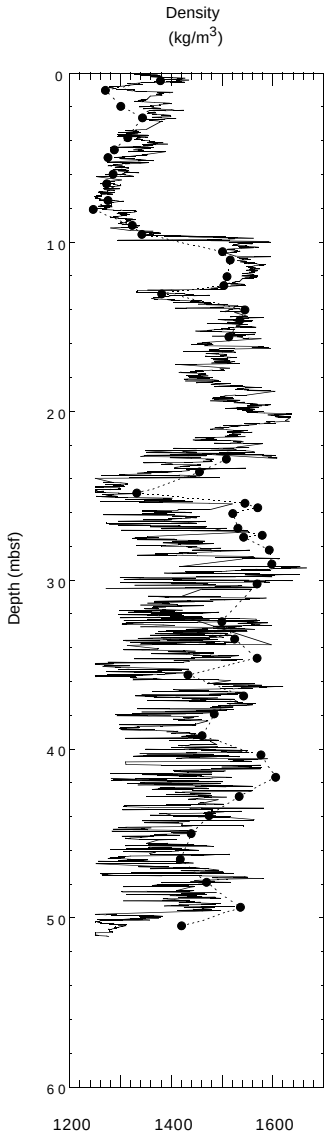

Figure 21. Discrete wet bulk density values (solid circles) compared with the GRAPE density profile (solid line) at Hole 1080A.

ties to the GRAPE and wet bulk density data are observed. High-quality discrete ultrasonic signals were recorded between 0 and 12 mbsf, but ended abruptly below 12 mbsf as a result of complete attenuation.

Index Properties

Results of discrete measurements of wet bulk density, porosity, and moisture content are presented in Figures 24A, 24B, and 24C, respectively (also see Table 11 on CD-ROM, back pocket, this volume). The density values vary between 1250 and 1610 kg/m^3. Porosity decreases from 82% in the top section to 62% at 52 mbsf (Fig. 24B), and moisture content varies between 68% and 40% from the top of Hole 1080A to 52 mbsf (Fig. 24C).

Thermal Conductivity

The thermal conductivity profile at Hole 1080A was determined in every second core section (see "Explanatory Notes" chapter, this volume). The values show a significant scatter and an overall decrease over the entire depth range (Fig. 22C). The thermal conductivity profile shows some positive correlation with porosity and undrained vane-shear strength.

Vane Shear Strength

An undrained vane-shear measurement was performed in the bottom part of each core section. The profile shows a pronounced increase in shear strength at 10 mbsf (Fig. 22D). A local maximum can be observed at 14 mbsf, which is followed by an overall decrease in shear strength. Core breaks are indicated in Figure 22D. As at previous sites, higher values of shear strength are found primarily in the middle sections of each core, probably the result of compressional and decompressional effects within the core barrel.

REFERENCES

Berggren, W.A., Kent, D.V., Swisher, C.C., III, and Aubry, M.-P., 1995. A revised Cenozoic geochronology and chronostratigraphy. *In* Berggren, W.A., Kent, D.V., Aubry, M.-P., and Hardenbol, J. (Eds.), *Geochronol-*

ogy, Time Scales and Global Stratigraphic Correlation. Spec. Publ.—Soc. Econ. Paleontol. Mineral. (Soc. Sediment. Geol.), 54:129–212.

Bleil, U., and Shipboard Scientific Party, 1995. Report and preliminary results of *SONNE* cruise SO 86. *Ber. Fachber. Geowiss*., Univ. Bremen, 51.

Bornhold, B.D., 1973. Late Quaternary sedimentation in the Eastern Angola Basin. *Tech. Rep. Woods Hole*, WHOI 73-8.

Cande, S., and Rabinowitz, P.D., 1978. Mesozoic sea floor spreading bordering conjugated continental margins of Angola and Brazil. *Proc. Offshore Tech. Conf.*, Rep. OTC 3268:1869–1876.

Claypool, G.E., and Kvenvolden, K.A., 1983. Methane and other hydrocarbon gases in marine sediment. *Annu. Rev. Earth Planet. Sci*., 11:299–327.

Duncombe Rae, C.M., Shillington, F.A., Agenbag, J.J., Taunton-Clark, J., and Gründling, M.L., 1992. An Agulhas ring in the South Atlantic Ocean and its interaction with the Benguela upwelling frontal system. *Deep-Sea Res.*, 39:1012–1033.

Embley, R.W., and Morley, J.J., 1980. Quaternary sedimentation and paleoenvironmental studies off Namibia (South-West Africa). *Mar. Geol.*, 36:183–204.

Emerson, S., and Hedges, J.I., 1988. Processes controlling the organic carbon content of open ocean sediments. *Paleoceanography*, 3:621–634.

Emery, K.O., Uchupi, E., Phillips, J., Bowin, C., and Mascle, J., 1975. Continental margin off Western Africa: Angola to Sierra Leone. *AAPG Bull.*, 59:2209–2265.

Harland, W.B., Armstrong, R.L., Cox, A.V., Craig, L.E., Smith, A.G., and Smith, D.G., 1990. *A Geologic Time Scale 1989:* Cambridge (Cambridge Univ. Press).

Hay, W.W., Sibuet, J.-C., et al., 1984. *Init. Repts. DSDP*, 75: Washington (U.S. Govt. Printing Office).

Kumar, N., 1979. Origin of paired aseismic rises: Ceará and Sierra Leone Rise in the Equatorial and the Rio Grande Rise and Walvis Ridge in the South Atlantic. *Mar. Geol.*, 30:175–191.

Little, M.G., Schneider, R.R., Kroon, D., Price, B., Bickert, T., and Wefer, G., 1997. Rapid paleoceanographic changes in the Benguela Upwelling System for the last 160,000 years as indicated by abundances of planktonic foraminifera. *Paleogeogr., Paleoclimatol., Palaeoecol.*, 130:135–161.

Locker, S., 1996. Cenozoic siliceous flagellates from the Fram Strait and the East Greenland Margin: biostratigraphic and paleoceanographic results. *In* Thiede, J., Myhre, A.M., Firth, J.V., Johnson, G.L., and Ruddiman, W.F. (Eds.), *Proc. ODP, Sci. Results*, 151: College Station, TX (Ocean Drilling Program), 101–124.

McIver, R.D., 1975. Hydrocarbon occurrences from JOIDES Deep Sea Drilling Project. *Proc. Ninth Petrol. Congr.*, 269–280.

Meyers, P.A., 1994. Preservation of elemental and isotopic source identification of sedimentary organic matter. *Chem. Geol.*, 144:289–302.

————, 1997. Organic geochemical proxies of paleoceanographic, paleolimnologic, and paleoclimatic processes. *Org. Geochem.*, 27:213–250.

Millero, F.J., and Sohn, M.L., 1992. *Chemical Oceanography:* Boca Raton (CRC Press).

Moore, T.C., Jr., 1995. Radiolarian stratigraphy, Leg 138. *In* Pisias, N.G., Mayer, L.A., Janecek, T.R., Palmer-Julson, A., and van Andel, T.H. (Eds.), *Proc. ODP, Sci. Results*, 138: College Station, TX (Ocean Drilling Program), 191–232.

Nelson, G., and Hutchins, L., 1983. The Benguela upwelling area. *Prog. Oceanogr.*, 12:333–356.

Peters, K.E., 1986. Guidelines for evaluating petroleum source rock using programmed pyrolysis. *AAPG Bull.*, 70:318–329.

Schell, I.I., 1970. Variability and persistence in the Benguela Current and upwelling off Southwest Africa. *J. Geophys. Res.*, 75:5225–5241.

Schneider, R., Dahmke, A., Kölling, A., Müller, P.J., Schulz, H.D., and Wefer, G., 1992. Strong deglacial minimum in the $\delta^{13}C$ record from planktonic foraminifera in the Benguela upwelling region: palaeoceanographic signal or early diagenetic imprint. *In* Summerhayes, C.P., Prell, W.L., Emeis, K.C. (Eds.), *Upwelling Systems: Evolution Since the Early Miocene.* Geol. Soc. Spec. Publ. London, 64:285–297.

Sibuet, J.-C., Hay, W.W., Prunier, A., Montadert, L., Hinz, K., and Fritsch, J., 1984. The eastern Walvis Ridge and adjacent basins (South Atlantic): morphology, stratigraphy and structural evolution in the light of the results of Legs 40 and 75. *In* Hay, W.W., Sibuet, J.-C., et al., *Init. Repts. DSDP*, 75: Washington (U.S. Govt. Printing Office), 483–508.

Stramma, L., and Peterson, R.G., 1989. Geostrophic transport in the Benguela Current region. *J. Phys. Oceanogr.*, 19:1440–1448.

Weaver, P.P.E., 1993. High resolution stratigraphy of marine Quaternary sequences. *In* Hailwood, E.A., and Kidd, R.B. (Eds.), *High Resolution Stratigraphy.* Geol. Soc. Spec. Publ. London, 70:137–153.

Wefer, G., and Shipboard Scientific Party, 1988. Bericht über die METEOR-Fahrt M6/6, Libreville - Las Palmas, 18.2–23.3. 1988. *Ber. Fachbereich Geowiss. Univ. Bremen, Germany*, 3.

Ms 175IR-108

NOTE: Core-description forms ("barrel sheets") and core photographs can be found in Section 4, beginning on page 219. Forms containing smear-slide data and can be found on CD-ROM. See Table of Contents for materials contained on CD-ROM.

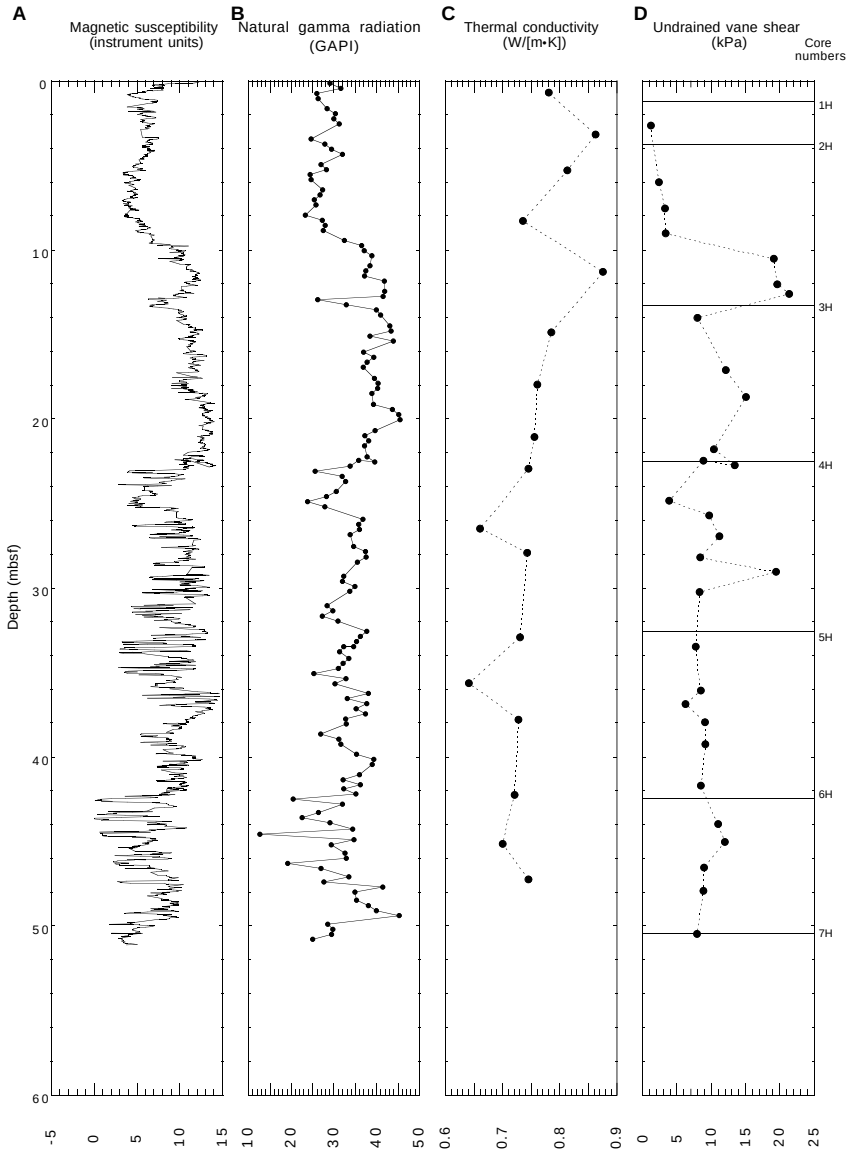

Figure 22. Plots of (**A**) magnetic susceptibility and (**B**) natural gamma radiation from MST measurements compared with discrete values of (**C**) thermal conductivity and (**D**) undrained vane shear strength at Hole 1080A.

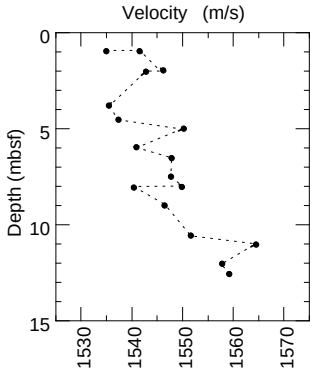

Figure 23. Discrete velocity profile measured at Hole 1080A.

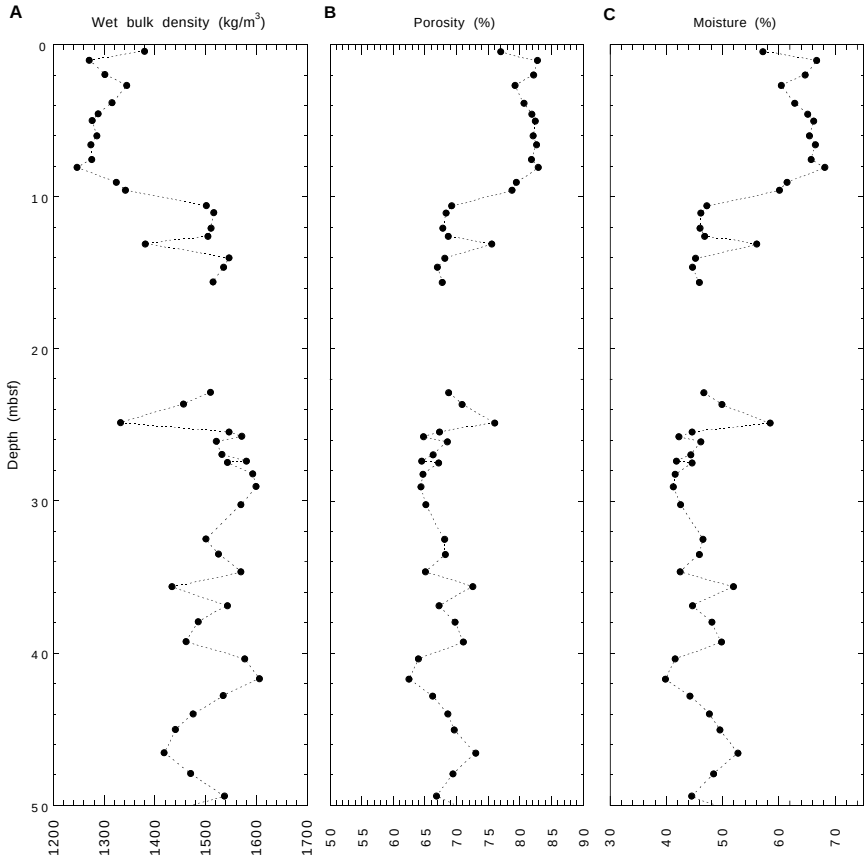

Figure 24. Plots of (**A**) wet bulk density, (**B**) porosity, and (**C**) moisture content derived from index properties measurements for Hole 1080A. No data = malfunction of measuring system.